DEPARTMENT OF MECHANICAL ENGINEERING

MECH0020 Individual Project

2019/20

Student:	**Suhayl Mehboob Patel**
Project Title:	**Optimisation of the mechanical design of a rotor head system in a small-scale helicopter using a kinematic model for a UAS Challenge Vehicle**
Supervisor:	**Dr Will Newton**

University College London
Torrington Place
LONDON WC1E 7JE

Optimisation of the mechanical design of a rotor head system in a small-scale helicopter using a kinematic model for a UAS Challenge Vehicle

Suhayl Mehboob Patel, Dr Will Newton

UCL Mechanical Engineering, Roberts Engineering Building (Room 4.11), Torrington Place, London WC1E 7JE, United Kingdom

Declaration

I, Suhayl Mehboob Patel, confirm that the work presented in this report is my own. Where information has been derived from other sources, I confirm that this has been indicated in the report.

Abstract

As part of the Institute of Mechanical Engineers (IMechE) Unmanned Aerial Systems (UAS) competition, students embark upon the challenge of designing and building an autonomous aerial system. This project focuses on the design and analysis of a rotor head system for an autonomous remote control (RC) helicopter, which will be UCL's entry to the 2021 competition.

The rotor head system is integral to the performance of a small-scale helicopter. When powered by a motor, the rotor head system produces thrust and enables a helicopter to roll and pitch. For the competition, it was uneconomical to manufacture a custom swashplate system and instead an existing rotor head system was bought to be integrated into a custom chassis and transmission design. This existing rotor head system was initially designed to be used in an Align T-Rex 550E Pro Direct Flight Controlled (DFC) RC helicopter.

To produce a complete rotor head system, the only remaining components that are to be added to the procured rotor head system are three servo motors, three servo horns and the accompanying linkages that connect them to the swashplate mechanism. However, the desired mounting positions for the servo motors, the servo horn lengths and the lengths of the linkages that are to be used are key factors for completing the design.

Autopilot systems that are used in autonomous RC helicopters use several sensing systems to determine the correct inputs to the rotor head system that produce the flight characteristics needed to fly a RC helicopter in a certain direction. However, before the advent of autopilot systems (such as Pixhawk and ArduPilot configurations), RC helicopters relied upon a robust mechanical design, that ensured the inputs from the servo motors in a rotor head system produce the required flight

characteristics. Therefore, in the worst-case scenario of a breakdown of the autopilot system, a good mechanical design of a rotor head system can provide a stable basis for a trained pilot or even a backup control system (that does not require the use of sensors), to make an emergency landing (called an autorotation).

As mentioned previously, the rotor head system that was purchased for UCL's 2021 entry is incomplete. To complete the design the position of three servo motors relative to the swashplate, the linkage lengths and the servo horn lengths need to be determined. Several prototypes can be used to determine the design parameters. On the other hand, this project provides a more efficient method to this design process. This project utilises the optimisation library in Microsoft Excel on a kinematic model of the rotor head system, to determine the design parameters for a new design that achieves the desired mechanical response so the system can be used with flight controllers. The nature of the desired response will be discussed later.

To gauge the impact of this method, the mechanical response of the new design is compared to the mechanical response of the rotor head system of the RC helicopter that the procured system was designed for. This is carried out by developing a 3D model of both systems and using MSC ADAMS to compare the two designs. To apply this design method, a kinematic analysis of the system was also developed. This project is beneficial for commercial RC helicopter designers, as it can influence their design process of new rotor head systems.

The MATLAB code and Microsoft Excel sheet developed have been submitted along with this report.

Acknowledgements

Indeed, all praise and thanks are due to God, whom without this project would have been impossible. I want to thank my family for their love and patience, without which I would have struggled to complete this project.

I would also like to express my gratitude towards my supervisor Dr Will Newton for being available to offer guidance throughout the project. I am grateful for his willingness to offer guidance and reminders to focus on the benefit of this project to the UAS community.

I am also very fortunate to have worked with Ismail Ahmed, a mentor from the performance and development team at UCL Racing, who provided a lot of inspiration and background knowledge to be able to work on the design of RC helicopters. I thank him for his willingness to teach and inspire the next generation of UAS team members at UCL.

I would also like to thank Professor Mohammad Reza Sabaapour and Professor Hassan Zohoor, who were open to discussion in regards to their paper on the kinematic analysis of a different model helicopter and from which the kinematic model derived in this project took huge inspiration from.

Table of Contents

Abbreviations:

IMechE	Institution of Mechanical Engineers
UAS	Unmanned Aerial System
RC	Remote Controlled
DFC	Direct Flight Controlled
AOA	Angle of Attack

List of Figures:

List of Tables:

1 Introduction:

1.1 Problem definition

As part of IMechE's UAS competition, the third-year team decided upon designing and building an autonomous remote control (RC) helicopter for the 2021 entry. A key part of the design is the rotor head system, which can produce thrust and enables a helicopter to roll and pitch. The key components to a rotor head system are servo motors, linkages, a swashplate mechanism, and the rotor blades. For the competition, it was uneconomical to manufacture a custom swashplate system and instead an existing rotor head system was bought to be integrated into a custom chassis and transmission design. This rotor head system was initially designed to be used in an Align T-Rex 550E Pro DFC RC helicopter and it is shown in Figure 1.

Figure 1.1: ALIGN T-Rex 550E Pro DFC rotor head system (1)

To produce a complete rotor head system, three servo motors, the servo horns and the accompanying linkages that connect them to the swashplate mechanism. However, the desired mounting positions for the servo motors and the lengths of the linkages that are to be used are key factors for completing the design. The choice of these parameters determines the mechanical response of the system and hence also affect the flight characteristics of the RC helicopter. A design is needed such that the system maximises a defined performance metric.

1.2 Aim and objectives

This project aims to apply the techniques used by past researchers on kinematic analysis to develop a mathematical representation of an RC helicopter rotor head system, and then use this derived model, to apply optimisation algorithms that can find the set of design parameters that enable the rotor head system to maximise a defined performance metric. These parameters will be used to produce a new design which will be compared to the mechanical response of the rotor head system of the RC helicopter that the procured system was designed for. This will be carried out by developing a 3D model of both systems and using CATIA V5 to compare the two designs.

1.3 Literature Review

Published works have developed kinematic models on rotor head systems in the past. Ref. (2) has developed a kinematic model for a coaxial helicopter's swashplate mechanism. However, this work was limited to the use of four actuators as inputs to the swashplate mechanism. This was not ideal as RC helicopter rotor head systems can function with only three actuators. Ref. (3) has developed a kinematic model for a PS-RRS-2RUS parallel manipulator. This manipulator is identical to the bottom half of a swashplate mechanism, and both the direct and inverse kinematic relations are derived for this system. However, the direct kinematic relations developed consider the prismatic joint to be one of the inputs to the system along with two revolute joints, instead of all three revolute joints being the inputs to the system, like in a RC helicopter rotor head system. Finally, the work of Sabaapour et al. (4) has provided a comprehensive kinematic analysis of the rotor head system in a model helicopter. However, their analysis is based upon an outdated design which consisted of a flybar. The flybar configurations of rotor head systems are no longer used in RC helicopters because of the advent of flybarless (FBL) controllers. (5)

The rotor head system shown in Figure 1 is a Direct Flight Control (DFC) design of the FBL rotor head. This design was chosen due to its mechanical simplicity, as compared to a non-integrated washout or integrated washout type FBL rotor head design. The alternative designs that could have been chosen are shown in Figure A.1 and Figure A.2 in Appendix A.

This paper will take inspiration from the kinematic models derived in the referenced works to develop a kinematic model for a DFC rotor head system.

1.4 The organisation of the thesis

This paper will begin with understanding the theory behind RC helicopter flight in Section 2. The success criteria for the new design will be defined in Section 3. A kinematic model and the explanation of the analysis will be done in Section 4. Section 5 will consist of the results and discussion. Finally, Section 6 will consist of the conclusion and suggestions for future work.

2 Theory on RC Helicopter Rotor Systems:

This section will discuss the relevant background reading carried out on RC helicopter rotor systems.

RC helicopter rotor systems can vary in complexity. The UAS team chose a Direct Flight Control (DFC) rotor head system with two main rotor blades. This will be the type of rotor head system that this report will focus on.

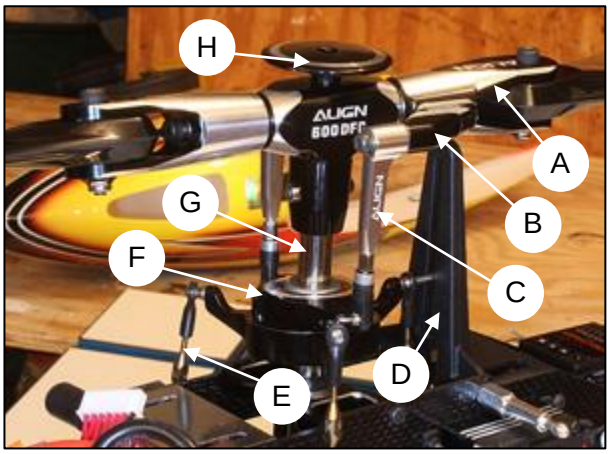

A. Main Rotor Holder
B. Main Rotor Holder Arm
C. DFC Main Rotor Link Arm
D. Anti-rotation Guide
E. Linkage Rod
F. Swashplate
G. Main Shaft
H. Headstopper

Figure 2.1: Direct flight control rotor head system. (6)

The main components of a DFC rotor head system are highlighted in Figure 2.1. The rotor blades of a collective pitch RC helicopter spin at a fixed revolutionary speed. By changing the angle of attack (AOA) of the main rotor blades, varying amounts of lift can be produced. The use of a swashplate mechanism bundled with at least three servo motors can control the AOA of the rotor blades. A swashplate has a fixed side and a rotating side, as shown in Figure 2.2.

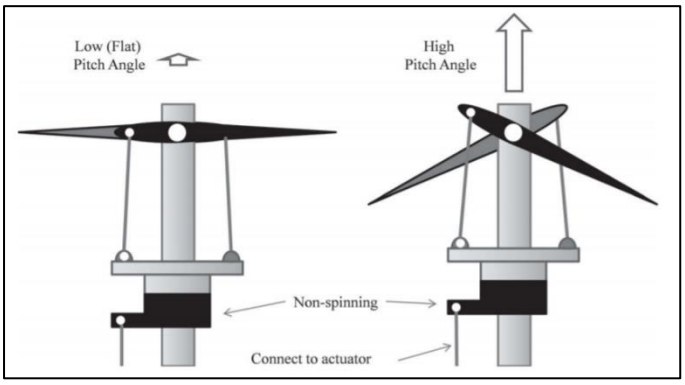

Figure 2.2: Collective pitch. (7)

The fixed side is connected to servo motors with linkage rods that pivot on several ball joints. Swashplates come in different configurations: with either four linkage rods placed 90° apart, or with three linkage rods placed in a triangular configuration. This allows the swashplate to rotate about two axes in its plane as well as being free to move in the direction parallel to the main shaft. (4)

Thrust magnitude control, or collective pitch, is achieved by moving each linkage symmetrically. Moving the swashplate up and down along the direction parallel to the main shaft changes the AoA of the rotor blades and increases the thrust. This is shown in Figure 2.2.

Being connected to at least three linkage rods also means the thrust vector can be tilted fore/aft and left/right. (7) This is called cyclic pitch, and it is achieved by tilting the swashplate.

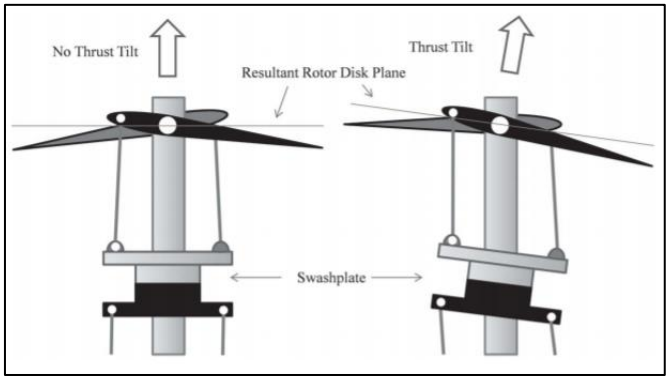

Figure 2.3: Cyclic pitch. (7)

As shown in Figure 2.3, by tilting the swashplate to the right, the blade reaches a maximum AOA when it is pointing out of the page, and when it is pointing into the page, it reaches a minimum AOA. This causes more thrust to be produced on the side pointing out of the page than the side pointing into the page. Due to the gyroscopic effect, this thrust imbalance causes the rotor to tilt to the right. (7) The tilt of the rotor disk plane produces a moment that can be used to achieve the desired rotation.

3 Success Criteria:

The transmitter pitch stick on RC helicopter radio transmitters controls the servo horn angle of each servo motor symmetrically, which enables the control of the blade pitch, as collective input. When the transmitter pitch stick is in the lowest position, the servo angle is the lowest negative value it can be (e.g. -25°); when it is in the middle position, the servo horn angle is 0°; and when it is in the highest position, the servo horn angle is in its highest position (with the same magnitude as the lowest position, e.g. 25°). Therefore, the throttle stick position translates to the servo horn angle. (8)

Flybarless flight controllers such as those produced by Futaba, perform best when the response of the helicopter to the initial input into the flight controller is proportional and linear to the maximum pitch, or roll rate. (9) A non-linear system is not ideal as this means the control algorithm of the flybarless system used, must compensate for this non-linear behaviour.

However, designing a helicopter that has a linear response has been a difficult. Figure 3.1 shows how various commercial RC helicopters perform in this regard.

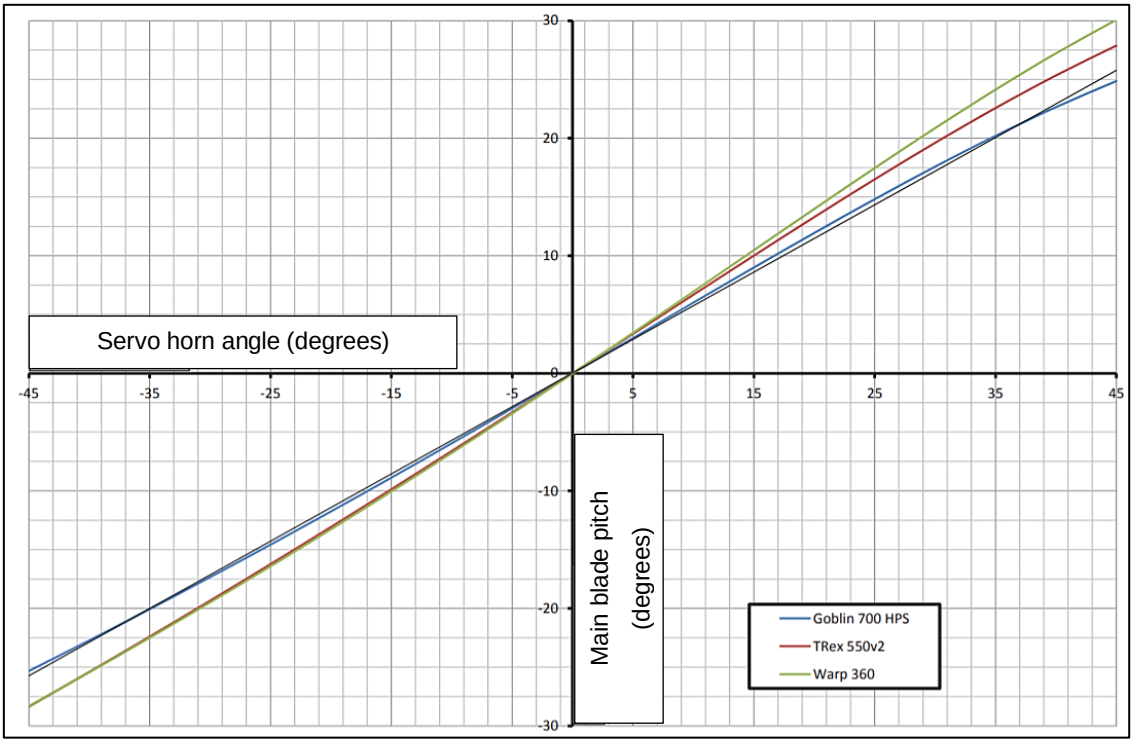

Figure 3.1: Comparison of pitch curve for various RC helicopters. (8)

Figure 3.2 shows the difference between the main blade pitch when the same servo angle is applied in the positive and negative direction for various helicopters. From Figure 3.2, one can see the impact of the design on the linearity of a system.

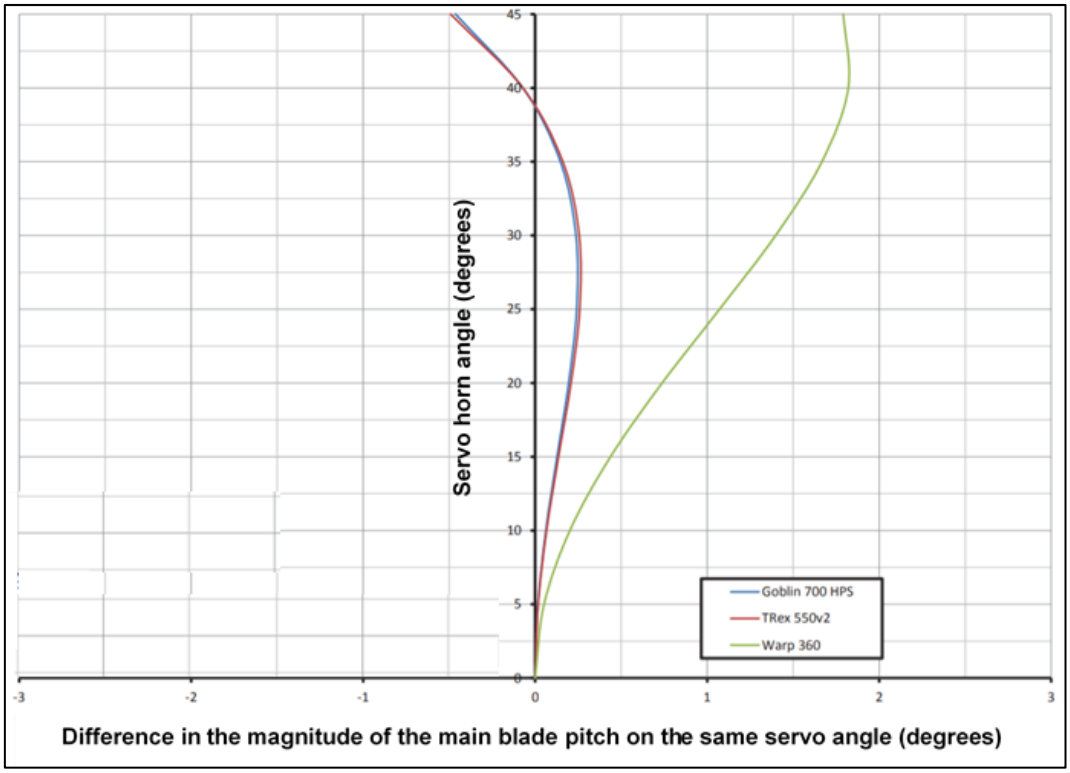

Figure 3.2: Effect of different designs on the pitch curve in both positive and negative AOA. (8)

Most RC helicopters operate in the range of -15° to 15°. Therefore, as shown by the green curve in Figure 3.2, a difference of approximately 0.8° is experienced by the Warp 360 RC helicopter at both 15° and -15°. The other commercial helicopters perform better. It is evident that different configurations of the rotor head system affect the pitch curve. From this we define the success criteria:

- The design minimises the pitch curve deviation from a linear response.
- The design has a more linear pitch curve than the pitch curve of the ALIGN T-REX 550E PRO DFC rotor head system, as the parts from this model are being utilised in the new design.

4 Kinematic Analysis:

In this section, a kinematic model for a DFC rotor head system is derived. This derivation takes great inspiration from the work of Sabaapour et al. shown in Ref. (4). Firstly, the rotor head system design of the Align T-Rex 550E Pro DFC will be analysed. Then, the design constraints are set, after which the strategy of analysis is explained. Finally, the model is derived.

4.1 Align T-Rex 550E Pro DFC rotor head system

Figure 4.1 and Figure 4.2 shows how the original system appears. The CAD model was sourced from Ref. (10) and was imported into CATIA V5 for analysis.

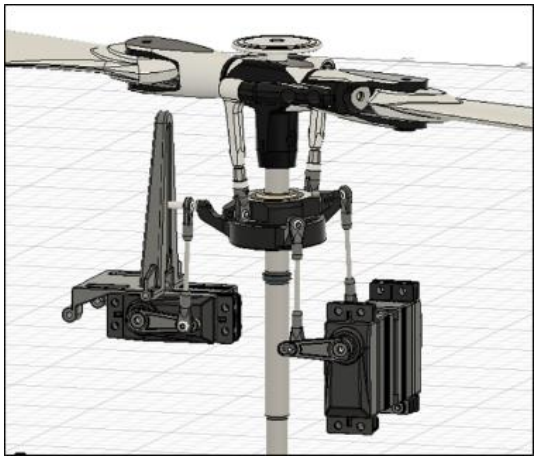

Figure 4.1: CAD model of Align T-Rex 550E Pro DFC rotor head system.

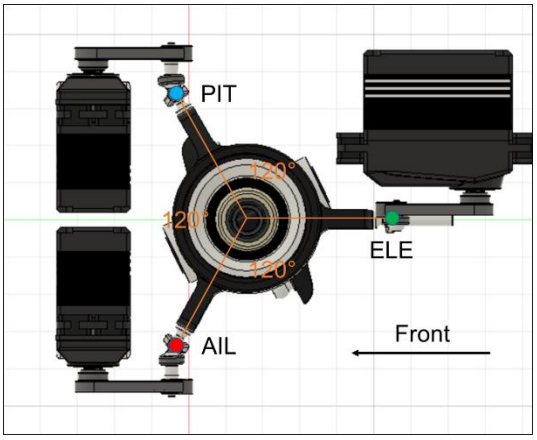

Figure 4.2: Bottom view of the swashplate mechanism and servo motor setup.

As evident in Figure 4.1 and Figure 4.2, the two front servos are aligned with the forward direction. This was most likely a design choice by the manufacturers of this helicopter, as placing them in this orientation allows the servos to be placed between two mounting plates. This means that their servo horns act at an angle to the arms of the swashplate (which are placed 120° apart) as shown in Figure 4.2. Though this arrangement is suitable, it leads to a sub-optimal force transfer between each servo horn and linkage rod of these servos as well as an unnecessary rotation of the linkage rods. Upon analysis of the model in CATIA V5, the pitch curve of the system for collective input was recorded and is shown in Figure 4.3 and Figure 4.4.

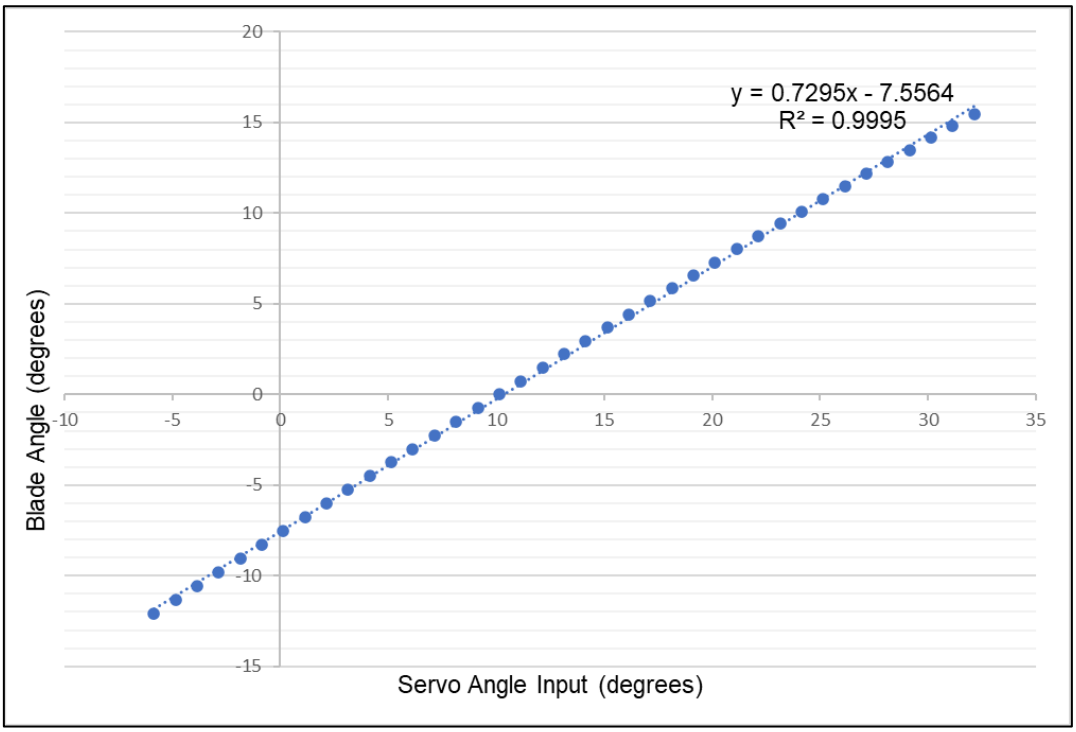

Figure 4.4: Align T-Rex 550E Pro DFC Collective Input Pitch Curve

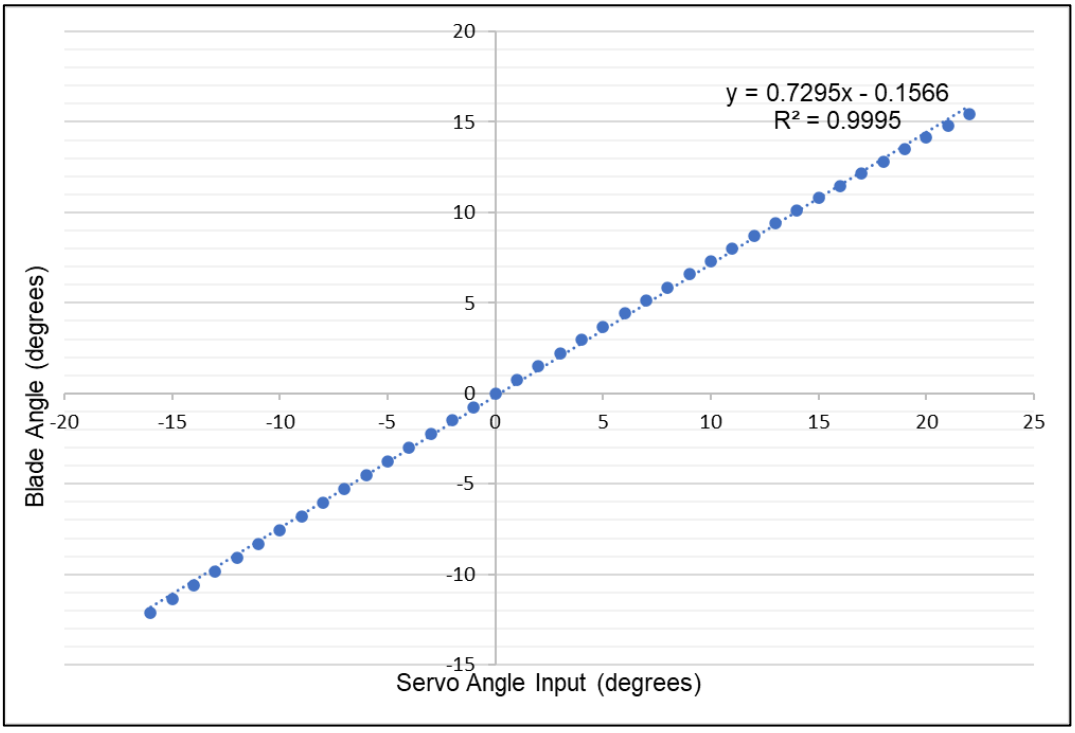

Figure 4.3: Align T-Rex 550E Pro DFC Collective Input Pitch Curve Normalised

Figure 4.3 shows the actual pitch curve. The setup has a pitch curve that is not symmetric about 0° servo input angle, but rather about a non-zero point which was 10.143°. Figure 4.4 shows the pitch curve normalised about this point. Figure 4.5 on the next page shows the difference between the main blade pitch when the same servo angle is applied in the positive and negative direction for various helicopters. The system could not go below -12° but it could achieve up to 15° in the positive pitch direction. Figure 4.5 shows that the difference in blade angle for the same input reaches -0.35° at 12° input.

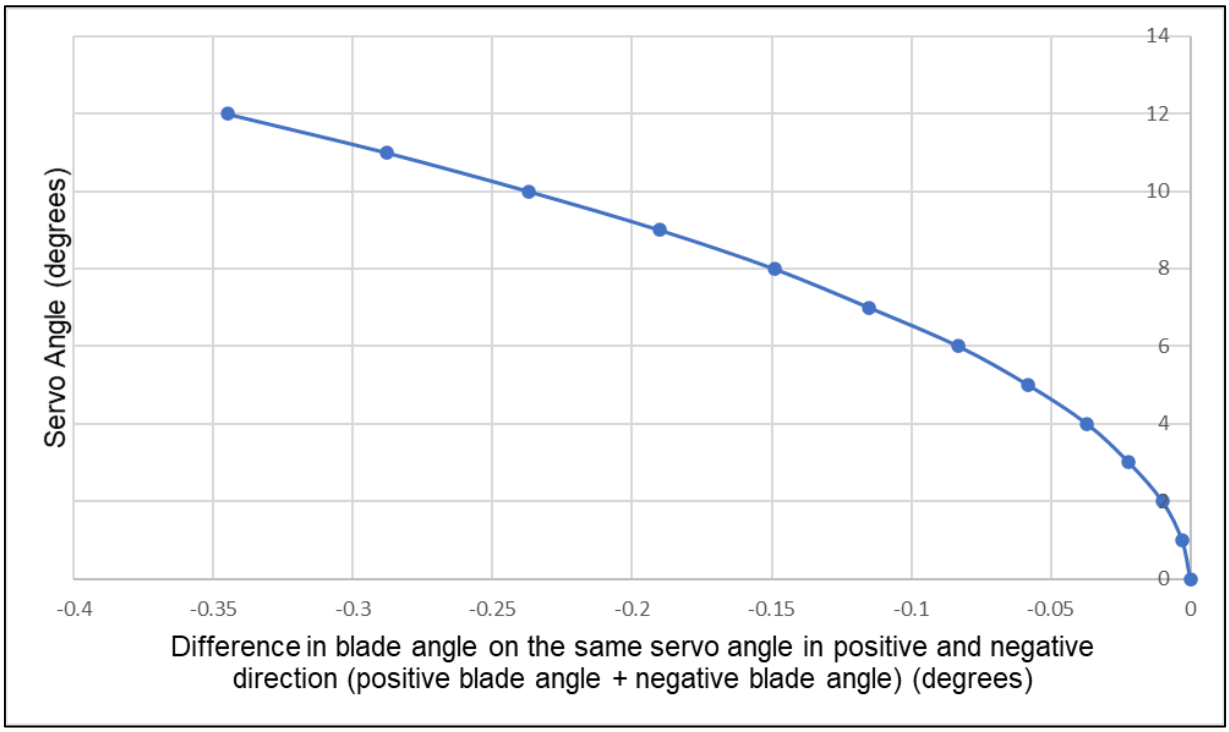

Figure 4.5: Comparison of the positive and negative regions of the pitch curve of Align T-Rex 550E Pro DFC.

These graphs show the baseline that the proposed design must be compared to.

4.2 Design Constraints

For the new design, the first design constraint is ensuring each servo is orientated such that the servo horns are aligned with the swashplate arms. As shown in Figure 4.2, the elevator servo is already orientated in this way.

Another aspect to consider is the direction that the servo horns turn with respect to the direction that the swashplate will tilt. In the current format, as shown in Figure 4.1, each of the servo horns rotates in an opposite direction to the tilt of the swashplate. This is sufficient for the operation of the system. However, there is a sub-optimal force transfer between the servo horns and the linkage rods. Therefore, each servo should be orientated such that the servo horn and swashplate rotation occur in the same direction.

Another constraint is that each servo horn will be in the mid position when the swashplate is level.

Each servo motor will also be constrained to use the same length servo horn, and linkage to connect to the relevant swashplate arm.

The final constraint is that each servo motor will be mounted on the same horizontal plane which is fixed. This enables each servo to be mounted onto one custom aluminium plate. Finally, the geometry of the swashplate system, the DFC arms and the rotor holders are fixed. With these in mind, a suitable configuration was found, and it is shown in Figure 4.6 and Figure 4.7. As shown in Figure 4.6 and Figure 4.7, each servo was oriented such that their servo horns line up with the swashplate arms.

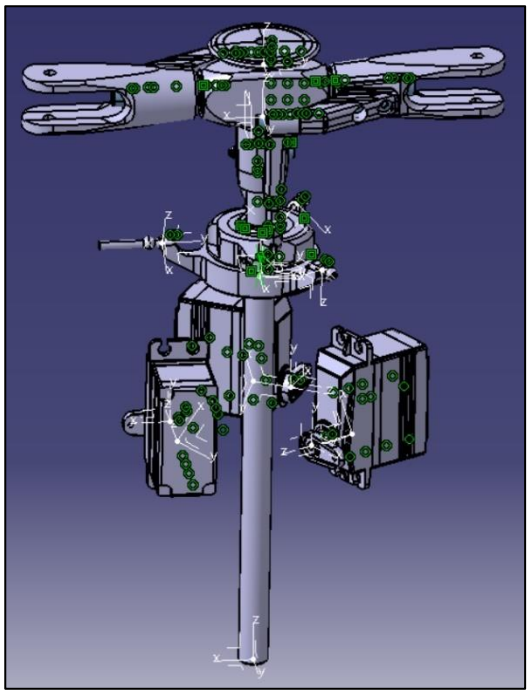

Figure 4.6: New proposed configuration.

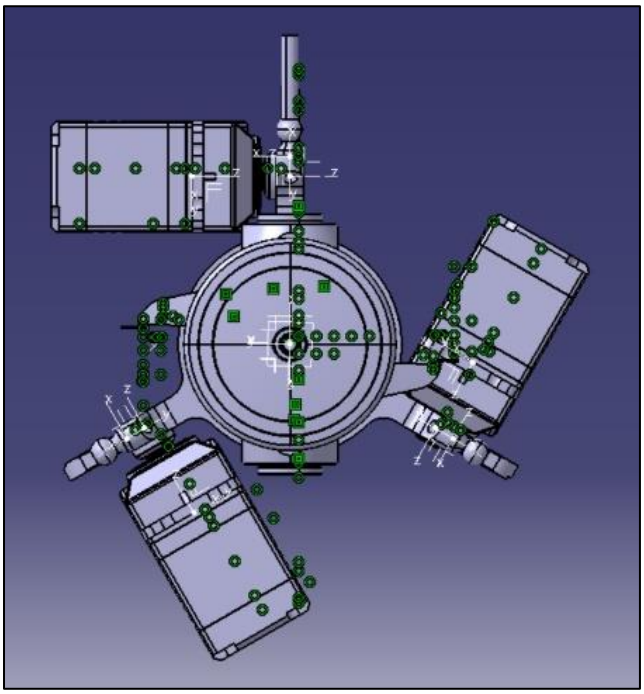

Figure 4.7: Top view of new configuration.

Note that the middle of the head stopper always remains at the same point. This gives the following parameters that can be altered:

- Servo horn length
- The distance of the servo pinion centre from the top of the head stopper
- The distance of the servo pinion centre from the main shaft axis
- Lengths of the linkage rods

The schematic of the whole system is shown in Figure 4.8.

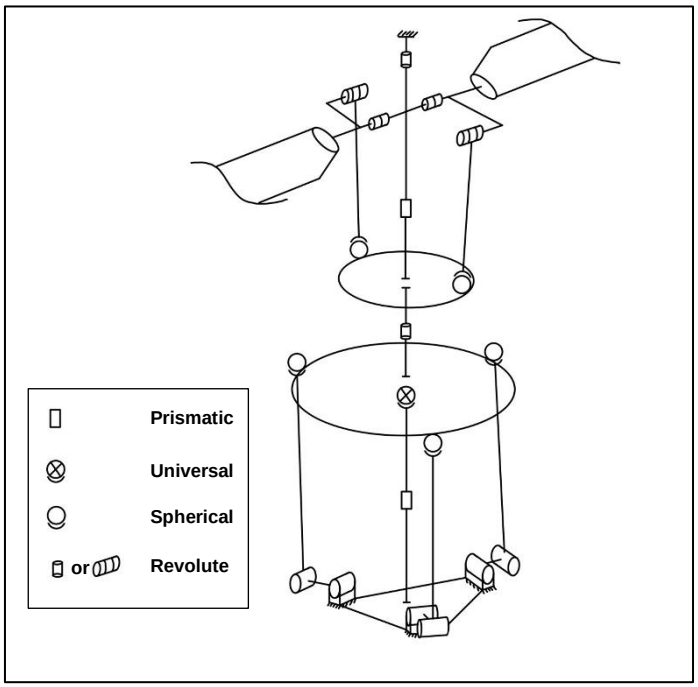

Figure 4.8: Schematic diagram of the new configuration.

4.3 Kinematic Analysis Strategy

A rotor head system has two parts. Using the terminology of Sabaapour et al., the system can be split into the Up-swashplate (Up – SP) module and the Down-swashplate module (Down – SP). (4)

The optimisation problem has the following objective function:

- Minimise the total difference between the ideal pitch curve and the actual pitch curve of the model.

Therefore, a global direct kinematic model is needed to calculate the actual pitch curve of a given design. Then, an optimisation algorithm can be applied with the above objective function to find a good set of design parameters. This strategy is summarised in Figure 4.9.

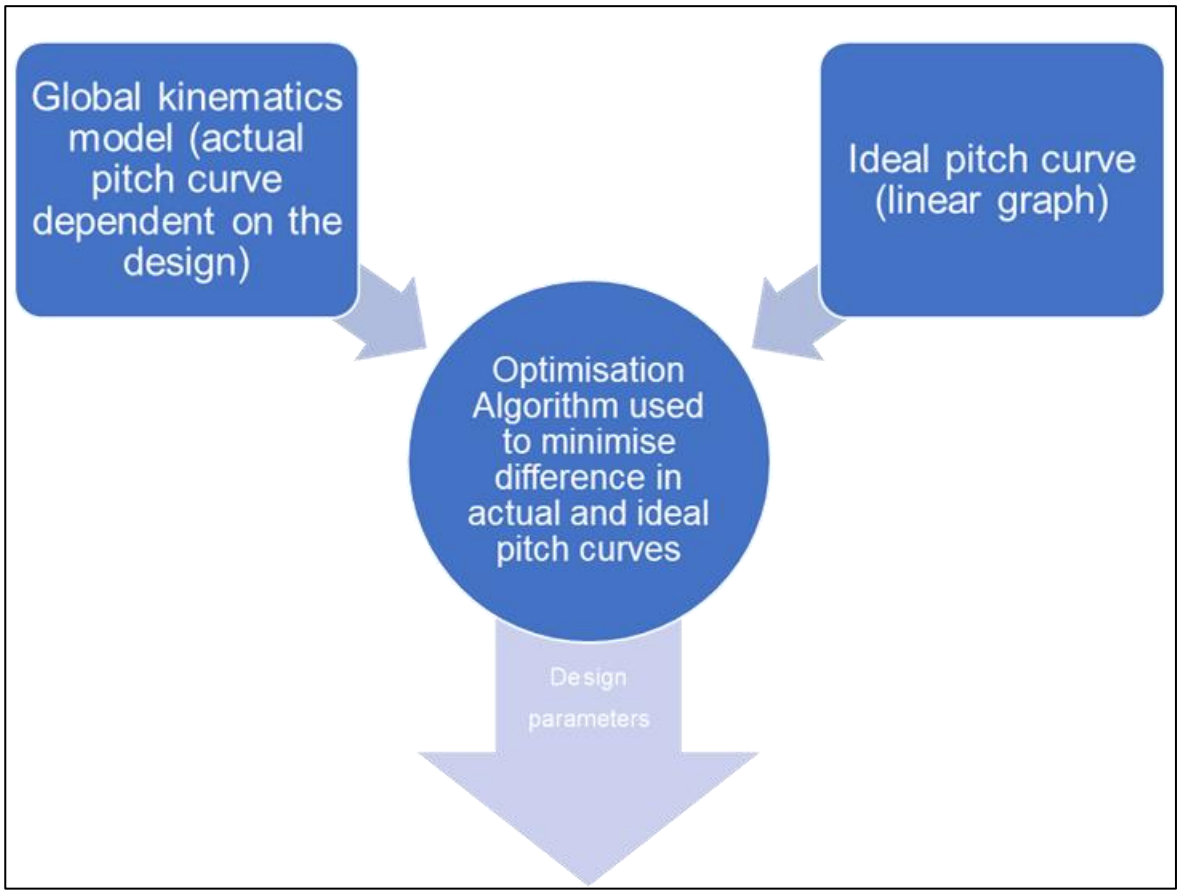

Figure 4.9: Strategy of analysis

4.4 Optimisation Algorithm

Microsoft (MS) Excel has the capability to implement a set of optimisation algorithms, that can be used to find the parameters that meet a specific objective function. The objective function for this problem is:

- Minimise the total difference between the ideal pitch curve and the actual pitch curve of the model.

MS Excel has three solving methods for a multi-constraint optimisation problem. These are:

- GRG Nonlinear
- Simplex LP
- Evolutionary

Since this is not a linear problem, the Simplex LP option is ruled out.

Allan Waren from Cleveland State University and Leon Lasdon from University of Texas at Austin developed the GRG solver, a nonlinear optimisation code. Being one of the most stable and efficient solutions to solving complex nonlinear programming problems, GRG and its particular implementation have been proved in practice for several years. (11)

On the other hand, genetic and evolutionary algorithms are used by the Evolutionary Solving approach to find solutions to non-smooth optimisation problems. This method is more robust at finding a global optimum to a problem and can avoid being fixated upon a local optimum. (12) This is possible because the solver can look for solutions from a population of initial inputs. The results from the population are compared, and a new set of test inputs are generated from the best performing input value (and this continues until there is an insignificant change in the value of the objective function). (13) However, this method can be very slow, and at times it can be difficult to decide on what to set maximum running times as. (14)

Since this optimisation problem relates to a design challenge, the calculated design parameters should be manufacturable. Therefore, this problem can be constrained to find only integer solutions. For this reason, the Evolutionary Solving approach was chosen.

4.5 Derivation of the model

4.5.1 Down – SP Module (direct kinematics)

The derivation for this section takes inspiration from the work of Sabaapour et al. (4) Their work lays out the steps taken to derive the kinematic model; however, the relevant workings are not shown. This paper will utilise these steps to derive the kinematic relationships as Sabaapour et al. had done but have not included in their paper.

Figure 4.10 illustrates a vector model of the Down – SP module. In the direct kinematics of this module, the three servo angles are provided, and the position of the fixed half of the swashplate is determined. First, the fixed reference frame is defined, passing through the centre of the triangular arrangement of the servo motors, which is point G (B-Frame). The X axis is aligned with one of the servo motors, whilst the Y axis points along the main rotor shaft. The position of the fixed section of the swashplate is characterised by its height off the ground, H, a rotation about the X axis (α) and a rotation about the Z axis (γ).

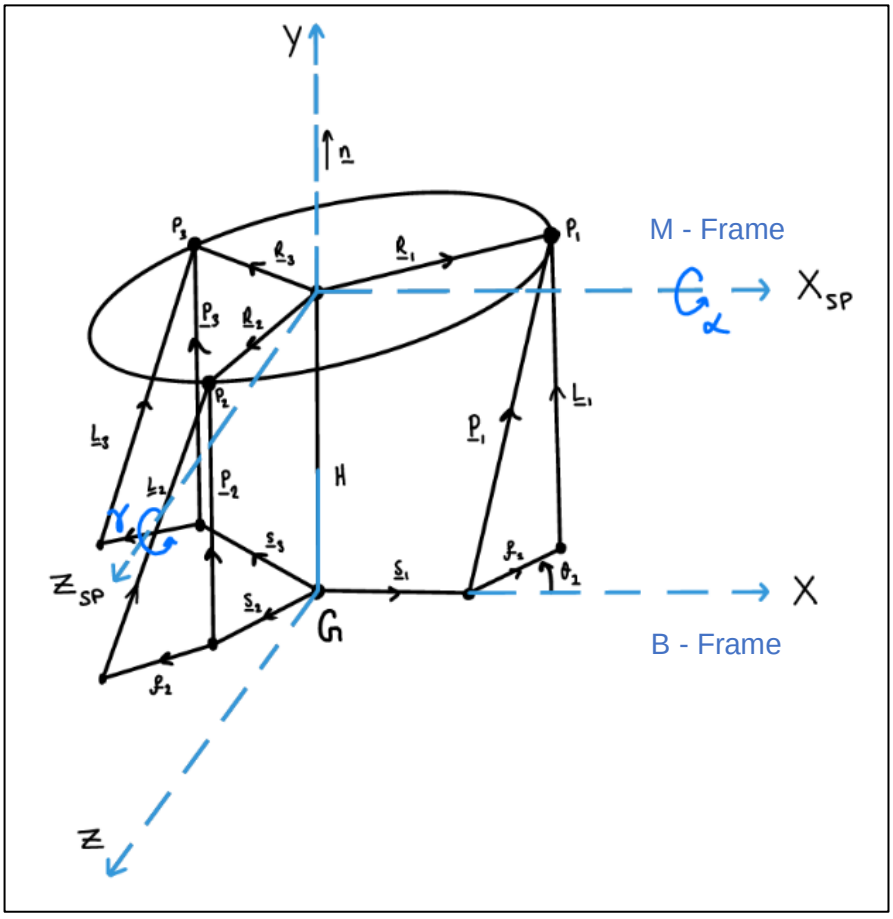

Figure 4.10: Vector representation of Down-SP module.

As done by Sabaapour et al., a loop closure equation can be written for each three of the actuator loops. (4)

$$\|\boldsymbol{\rho_i} - \boldsymbol{P_i}\|^2 = \|\boldsymbol{L_i}\|^2 = {l_i}^2 \qquad \textit{Equation 1}$$

But,

$$\boldsymbol{P_i} = H\boldsymbol{n} + \boldsymbol{R_i} - \boldsymbol{s_i} \qquad \textit{Equation 2}$$

Substituting Eq. 2 into Eq. 1 and simplifying gives:

$$\begin{aligned} {l_i}^2 &= \|\boldsymbol{\rho_i} - H\boldsymbol{n} - \boldsymbol{R_i} + \boldsymbol{s_i}\|^2 \\ &= (\boldsymbol{\rho_i} - H\boldsymbol{n} - \boldsymbol{R_i} + \boldsymbol{s_i})^{\mathrm{T}}(\boldsymbol{\rho_i} - H\boldsymbol{n} - \boldsymbol{R_i} + \boldsymbol{s_i}) = {l_i}^2 \\ &= \rho_i^2 - H\boldsymbol{\rho_i}^{\mathrm{T}}\boldsymbol{n} - \boldsymbol{\rho_i}^{\mathrm{T}}\boldsymbol{R_i} + \boldsymbol{\rho_i}^{\mathrm{T}}\boldsymbol{s_i} - H\boldsymbol{n}^{\mathrm{T}}\boldsymbol{\rho_i} + H^2 + H\boldsymbol{n}^{\mathrm{T}}\boldsymbol{R_i} - H\boldsymbol{n}^{\mathrm{T}}\boldsymbol{s_i} - \boldsymbol{R_i}^{\mathrm{T}}\boldsymbol{\rho_i} + H\boldsymbol{R_i}^{\mathrm{T}}\boldsymbol{n} \\ &\qquad + R^2 - \boldsymbol{R_i}^{\mathrm{T}}\boldsymbol{s_i} + \boldsymbol{s_i}^{\mathrm{T}}\boldsymbol{\rho_i} - H\boldsymbol{s_i}^{\mathrm{T}}\boldsymbol{n} - \boldsymbol{s_i}^{\mathrm{T}}\boldsymbol{R_i} + s_i^2 \\ &= \rho_i^2 + H^2 + R_i^2 + s_i^2 - H\boldsymbol{\rho_i}^{\mathrm{T}}\boldsymbol{n} - H\boldsymbol{n}^{\mathrm{T}}\boldsymbol{\rho_i} - \boldsymbol{\rho_i}^{\mathrm{T}}\boldsymbol{R_i} - \boldsymbol{R_i}^{\mathrm{T}}\boldsymbol{\rho_i} + \boldsymbol{\rho_i}^{\mathrm{T}}\boldsymbol{s_i} + \boldsymbol{s_i}^{\mathrm{T}}\boldsymbol{\rho_i} + H\boldsymbol{n}^{\mathrm{T}}\boldsymbol{R_i} \\ &\qquad + H\boldsymbol{R_i}^{\mathrm{T}}\boldsymbol{n} - H\boldsymbol{n}^{\mathrm{T}}\boldsymbol{s_i} - H\boldsymbol{s_i}^{\mathrm{T}}\boldsymbol{n} - \boldsymbol{R_i}^{\mathrm{T}}\boldsymbol{s_i} - \boldsymbol{s_i}^{\mathrm{T}}\boldsymbol{R_i} \end{aligned} \qquad \textit{Equation 3}$$

Since this system is dealing with vectors of size 3×1, Eq. 3 can be simplified to:

$$\begin{aligned} {l_i}^2 &= \rho_i^2 + H^2 + R_i^2 + s_i^2 - 2H\boldsymbol{n}^{\mathrm{T}}\boldsymbol{\rho_i} - 2\boldsymbol{\rho_i}^{\mathrm{T}}\boldsymbol{R_i} + 2\boldsymbol{s_i}^{\mathrm{T}}\boldsymbol{\rho_i} + 2H\boldsymbol{n}^{\mathrm{T}}\boldsymbol{R_i} - 2H\boldsymbol{n}^{\mathrm{T}}\boldsymbol{s_i} - 2\boldsymbol{s_i}^{\mathrm{T}}\boldsymbol{R_i} \\ &= \rho_i^2 + H^2 + R_i^2 + s_i^2 - 2H\boldsymbol{n}^{\mathrm{T}}\boldsymbol{\rho_i} + 2H\boldsymbol{n}^{\mathrm{T}}\boldsymbol{R_i} - 2H\boldsymbol{n}^{\mathrm{T}}\boldsymbol{s_i} + 2\boldsymbol{s_i}^{\mathrm{T}}\boldsymbol{\rho_i} - 2\boldsymbol{s_i}^{\mathrm{T}}\boldsymbol{R_i} - 2\boldsymbol{\rho_i}^{\mathrm{T}}\boldsymbol{R_i} \\ &= \rho_i^2 + H^2 + R_i^2 + s_i^2 - 2H\boldsymbol{n}^{\mathrm{T}}(\boldsymbol{\rho_i} + \boldsymbol{s_i} - \boldsymbol{R_i}) + 2\boldsymbol{s_i}^{\mathrm{T}}(\boldsymbol{\rho_i} - \boldsymbol{R_i}) - 2\boldsymbol{\rho_i}^{\mathrm{T}}\boldsymbol{R_i} \end{aligned} \qquad \textit{Equation 4}$$

Bringing all the terms to one side gives:

$$0 = -{l_i}^2 + \rho_i^2 + H^2 + R_i^2 + s_i^2 - 2H\boldsymbol{n}^{\mathrm{T}}(\boldsymbol{\rho_i} + \boldsymbol{s_i} - \boldsymbol{R_i}) + 2\boldsymbol{s_i}^{\mathrm{T}}(\boldsymbol{\rho_i} - \boldsymbol{R_i}) - 2\boldsymbol{\rho_i}^{\mathrm{T}}\boldsymbol{R_i} \qquad \textit{Equation 5}$$

The constants c_i, A_i and B_i can be defined as follows:

$$c_i = -{l_i}^2 + \rho_i^2 + R_i^2 + s_i^2$$

$$A_i = -2\boldsymbol{n}^{\mathrm{T}}(\boldsymbol{\rho_i} + \boldsymbol{s_i} - \boldsymbol{R_i})$$

$$B_i = 2\boldsymbol{s_i}^{\mathrm{T}}(\boldsymbol{\rho_i} - \boldsymbol{R_i}) - 2\boldsymbol{\rho_i}^{\mathrm{T}}\boldsymbol{R_i} + c_i$$

Applying this to Eq. 5 gives:

$$\begin{aligned} 0 &= H^2 - 2H\boldsymbol{n}^{\mathrm{T}}(\boldsymbol{\rho_i} + \boldsymbol{s_i} - \boldsymbol{R_i}) + 2\boldsymbol{s_i}^{\mathrm{T}}(\boldsymbol{\rho_i} - \boldsymbol{R_i}) - 2\boldsymbol{\rho_i}^{\mathrm{T}}\boldsymbol{R_i} + c_i \\ 0 &= H^2 + A_iH + B_i \quad ; \quad i = 1, 2, 3 \end{aligned} \qquad \textit{Equation 6}$$

Multiplying Eq. 6 gives:

$$0 = H^3 + A_iH^2 + B_iH \quad ; \quad i = 1, 2, 3 \qquad \textit{Equation 7}$$

As shown by Sabaapour et al., Eq. 6 and Eq. 7 together can be written as two homogeneous matrix equations. (4) For $i = 1$ and $i = 2$, Eq. 6 and Eq. 7 can be used to give:

$$\boldsymbol{M_1 x} = 0 \quad \text{Where,} \quad \boldsymbol{M_1} = \begin{bmatrix} 0 & 1 & A_1 & B_1 \\ 0 & 1 & A_2 & B_2 \\ 1 & A_1 & B_1 & 0 \\ 1 & A_2 & B_2 & 0 \end{bmatrix} \quad \text{and,} \quad \boldsymbol{x} = \begin{bmatrix} H^3 \\ H^2 \\ H \\ 1 \end{bmatrix} \qquad \textit{Equation 8}$$

For $i = 2$ and $i = 3$, Eq. 6 and Eq. 7 can be used to give:

$$\boldsymbol{M_2 x} = 0 \quad \text{Where,} \quad \boldsymbol{M_2} = \begin{bmatrix} 0 & 1 & A_2 & B_2 \\ 0 & 1 & A_3 & B_3 \\ 1 & A_2 & B_3 & 0 \\ 1 & A_3 & B_3 & 0 \end{bmatrix} \quad \text{and,} \quad \boldsymbol{x} = \begin{bmatrix} H^3 \\ H^2 \\ H \\ 1 \end{bmatrix} \qquad \textit{Equation 9}$$

As mentioned by Sabaapour et al., the determinants of $\boldsymbol{M_1}$ and $\boldsymbol{M_2}$, must equal zero if there is to be a nontrivial solution. (4) They write:

$$\det(\boldsymbol{M_1}) = f_1(\alpha,\gamma) = 0 \qquad \textit{Equation 10}$$

$$\det(\boldsymbol{M_2}) = f_2(\alpha,\gamma) = 0 \qquad \textit{Equation 11}$$

Eq. 10 can be evaluated to give:

$$\begin{aligned} 0 &= -B_1^2 - B_1A_2^2 + A_1B_1A_2 + 2B_1B_2 - B_2^2 + A_1A_2B_2 - A_1^2B_2 \\ &= A_1A_2(B_1+B_2) - B_1(A_2^2+B_1) - B_2(A_1^2+B_2) + 2B_1B_2 \end{aligned} \qquad \text{Equation 12}$$

Eq. 11 can be evaluated to give:

$$\begin{aligned} 0 &= -B_2^2 - B_2A_3^2 + A_2B_2A_3 + 2B_2B_3 - B_3^2 + A_2A_3B_3 - A_2^2B_3 \\ &= A_2A_3(B_2+B_3) - B_2(A_3^2+B_2) - B_3(A_2^2+B_3) + 2B_2B_3 \end{aligned} \qquad \textit{Equation 13}$$

To solve for the unknowns, A_i and B_i for $i = 1, 2, 3$ must be determined in terms of α and γ. This will now be dealt with. For ease, from now on, $\cos\theta = c(\theta)$ and $\sin\theta = s(\theta)$.

To achieve this, the vector definitions of each vector is needed, as measured from the fixed reference frame. All are known, except $\boldsymbol{R_1}$, $\boldsymbol{R_2}$ and $\boldsymbol{R_3}$, which are only known in the reference frame attached to the fixed half of the swashplate.

Using rotation matrices $\boldsymbol{R_1}$, $\boldsymbol{R_2}$ and $\boldsymbol{R_3}$ can be defined in terms of the fixed reference frame. By referring to Figure 4.10, it is evident that:

$$\begin{aligned} {}^{\{B\}}\overrightarrow{OP_1} = {}^{\{B\}}\boldsymbol{R_1} &= {}^{\{B\}}_{\{M\}}\boldsymbol{R_Z}\,{}^{\{M\}}\boldsymbol{R_1} \\ &= \begin{bmatrix} c(\gamma) & -s(\gamma) & 0 \\ s(\gamma) & c(\gamma) & 0 \\ 0 & 0 & 1 \end{bmatrix}\begin{bmatrix} R_1 \\ 0 \\ 0 \end{bmatrix} = \begin{bmatrix} R_1c(\gamma) \\ R_1s(\gamma) \\ 0 \end{bmatrix} \\ {}^{\{B\}}\overrightarrow{OP_2} = {}^{\{B\}}\boldsymbol{R_2} &= {}^{\{B\}}_{\{M\}}\boldsymbol{R_Z}\,{}^{\{B\}}_{\{M\}}\boldsymbol{R_X}\,{}^{\{M\}}\boldsymbol{R_2} \\ &= \begin{bmatrix} c(\gamma) & -s(\gamma) & 0 \\ s(\gamma) & c(\gamma) & 0 \\ 0 & 0 & 1 \end{bmatrix}\begin{bmatrix} 1 & 0 & 0 \\ 0 & c(\alpha) & -s(\alpha) \\ 0 & s(\alpha) & c(\alpha) \end{bmatrix}\begin{bmatrix} -\frac{1}{2}R_2 \\ 0 \\ \frac{\sqrt{3}}{2}R_2 \end{bmatrix} \\ &= \begin{bmatrix} c(\gamma) & -s(\gamma)c(\alpha) & s(\gamma)s(\alpha) \\ s(\gamma) & c(\gamma)c(\alpha) & -c(\gamma)s(\alpha) \\ 0 & s(\alpha) & c(\alpha) \end{bmatrix}\begin{bmatrix} -\frac{1}{2}R_2 \\ 0 \\ \frac{\sqrt{3}}{2}R_2 \end{bmatrix} \\ &= \begin{bmatrix} -\frac{1}{2}R_2c(\gamma) + \frac{\sqrt{3}}{2}R_2s(\gamma)s(\alpha) \\ -\frac{1}{2}R_2s(\gamma) - \frac{\sqrt{3}}{2}R_2c(\gamma)s(\alpha) \\ \frac{\sqrt{3}}{2}R_2c(\alpha) \end{bmatrix} \end{aligned}$$

$$
\begin{aligned}
{}^{\{B\}}\overrightarrow{OP_3} = {}^{\{B\}}\boldsymbol{R_3} = {}& {}^{\{B\}}_{\{M\}}\boldsymbol{R_Z}\,{}^{\{B\}}_{\{M\}}\boldsymbol{R_X}\,{}^{\{M\}}\boldsymbol{R_3} \\
= {}& \begin{bmatrix} c(\gamma) & -s(\gamma)c(\alpha) & s(\gamma)s(\alpha) \\ s(\gamma) & c(\gamma)c(\alpha) & -c(\gamma)s(\alpha) \\ 0 & s(\alpha) & c(\alpha) \end{bmatrix} \begin{bmatrix} -\frac{1}{2}R_3 \\ 0 \\ -\frac{\sqrt{3}}{2}R_3 \end{bmatrix} \\
= {}& \begin{bmatrix} -\frac{1}{2}R_3 c(\gamma) - \frac{\sqrt{3}}{2}R_3 s(\gamma)s(\alpha) \\ -\frac{1}{2}R_3 s(\gamma) + \frac{\sqrt{3}}{2}R_3 c(\gamma)s(\alpha) \\ -\frac{\sqrt{3}}{2}R_3 c(\alpha) \end{bmatrix}
\end{aligned}
$$

Where Zhang et al. define ${}^{\{B\}}_{\{M\}}\boldsymbol{R_Z}$ and ${}^{\{B\}}_{\{M\}}\boldsymbol{R_X}$ as the rotation matrices that define the first and second rotations of the bottom half of the swashplate with respect to the B-frame whilst following the Euler angle convention, where angles γ and α, represent the first and second rotations about the Z axis and a rotation about the X axis, respectively. (3)

Returning to the definitions of A_i and B_i for $i = 1, 2, 3$, to simplify the relations, the following half-tangent relations are used:

$$s(\gamma) = \frac{2t_\gamma}{1+t_\gamma^2}, \qquad c(\gamma) = \frac{1-t_\gamma^2}{1+t_\gamma^2}, \qquad \text{Where, } t_\gamma = \tan\left(\frac{\gamma}{2}\right)$$

$$s(\alpha) = \frac{2t_\alpha}{1+t_\alpha^2}, \qquad c(\alpha) = \frac{1-t_\alpha^2}{1+t_\alpha^2}, \qquad \text{Where, } t_\alpha = \tan\left(\frac{\alpha}{2}\right)$$

Also, due to the constraints defined in Section 4.2:

$$R_1 = R_2 = R_3 = R$$
$$\rho_1 = \rho_2 = \rho_3 = \rho$$
$$l_1 = l_2 = l_3 = l$$
$$s_1 = s_2 = s_3 = s$$

Firstly, by referring to Figure 4.10, A_1 is determined, by substituting the relevant vectors measured in the reference coordinate system into the definition for A_1.

$$
\begin{aligned}
A_1 = {}& -2\boldsymbol{n}^{\mathrm{T}}(\boldsymbol{\rho_1} + \boldsymbol{s_1} - \boldsymbol{R_1}) \\
= {}& -2[0 \quad 1 \quad 0]\left(\begin{bmatrix} \rho_1 c(\theta_1) \\ \rho_1 s(\theta_1) \\ 0 \end{bmatrix} + \begin{bmatrix} s_1 \\ 0 \\ 0 \end{bmatrix} - \begin{bmatrix} R_1 c(\gamma) \\ R_1 s(\gamma) \\ 0 \end{bmatrix}\right) \\
= {}& [0 \quad -2 \quad 0]\begin{bmatrix} \rho_1 c(\theta_1) + s_1 - R_1 c(\gamma) \\ \rho_1 s(\theta_1) - R_1 s(\gamma) \\ 0 \end{bmatrix} = -2\big(\rho_1 s(\theta_1) - R_1 s(\gamma)\big) \\
= {}& -2\rho_1 s(\theta_1) + 4R_1\left(\frac{t_\gamma}{1+t_\gamma^2}\right) = -2\rho s(\theta_1) + 4R\left(\frac{t_\gamma}{1+t_\gamma^2}\right)
\end{aligned}
$$

Next, B_1 is determined:

$$
\begin{aligned}
B_1 = \;& 2\boldsymbol{s_i}^{\mathrm{T}}(\boldsymbol{\rho_i} - \boldsymbol{R_i}) - 2\boldsymbol{\rho_i}^{\mathrm{T}}\boldsymbol{R_i} + c_i \\
= \;& 2[s_1 \quad 0 \quad 0]\left(\begin{bmatrix}\rho_1 c(\theta_1)\\ \rho_1 s(\theta_1)\\ 0\end{bmatrix} - \begin{bmatrix}R_1 c(\gamma)\\ R_1 s(\gamma)\\ 0\end{bmatrix}\right) - 2[\rho_1 c(\theta_1) \quad \rho_1 s(\theta_1) \quad 0]\begin{bmatrix}R_1 c(\gamma)\\ R_1 s(\gamma)\\ 0\end{bmatrix} + c_1 \\
= \;& 2s_1\big(\rho_1 c(\theta_1) - R_1 c(\gamma)\big) - 2\big(\rho_1 R_1 c(\theta_1)c(\gamma) + \rho_1 R_1 s(\theta_1)s(\gamma)\big) + c_1 \\
= \;& -2\rho_1 R_1 c(\theta_1)c(\gamma) - 2s_1 R_1 c(\gamma) - 2\rho_1 R_1 s(\theta_1)s(\gamma) + 2s_1\rho_1 c(\theta_1) + c_1 \\
= \;& -2R_1 c(\gamma)(\rho_1 c(\theta_1) + s_1) - 2\rho_1 R_1 s(\theta_1)s(\gamma) + 2s_1\rho_1 c(\theta_1) + c_1 \\
= \;& -2R_1(\rho_1 c(\theta_1) + s_1)\left(\frac{1 - t_\gamma^2}{1 + t_\gamma^2}\right) - 2\rho_1 R_1 s(\theta_1)\left(\frac{2t_\gamma}{1 + t_\gamma^2}\right) + 2s_1\rho_1 c(\theta_1) + c_1 \\
= \;& \left(\frac{-2R_1(\rho_1 c(\theta_1) + s_1)\big(1 - t_\gamma^2\big) - 4\rho_1 R_1 s(\theta_1)t_\gamma}{1 + t_\gamma^2}\right) + 2s_1\rho_1 c(\theta_1) + c_1 \\
= \;& \left(\frac{-2R(\rho c(\theta_1) + s)\big(1 - t_\gamma^2\big) - 4\rho R s(\theta_1)t_\gamma}{1 + t_\gamma^2}\right) + 2s\rho c(\theta_1) - l^2 + \rho + R^2 + s^2
\end{aligned}
$$

Next, A_2 is determined:

$$
\begin{aligned}
A_2 = \;& -2\boldsymbol{n}^{\mathrm{T}}(\boldsymbol{\rho_2} + \boldsymbol{s_2} - \boldsymbol{R_2}) \\
= \;& -2[0 \quad 1 \quad 0]\left(\begin{bmatrix}-\frac{1}{2}\rho_2 c(\theta_2)\\ \rho_2 s(\theta_2)\\ \frac{\sqrt{3}}{2}\rho_2 c(\theta_2)\end{bmatrix} + \begin{bmatrix}-\frac{1}{2}s_2\\ 0\\ \frac{\sqrt{3}}{2}s_2\end{bmatrix} - \begin{bmatrix}-\frac{1}{2}R_2 c(\gamma) + \frac{\sqrt{3}}{2}R_2 s(\gamma)s(\alpha)\\ -\frac{1}{2}R_2 s(\gamma) - \frac{\sqrt{3}}{2}R_2 c(\gamma)s(\alpha)\\ \frac{\sqrt{3}}{2}R_2 c(\alpha)\end{bmatrix}\right) \\
= \;& [0 \quad -2 \quad 0]\begin{bmatrix}-\frac{1}{2}\rho_2 c(\theta_2) - \frac{1}{2}s_2 + \frac{1}{2}R_2 c(\gamma) - \frac{\sqrt{3}}{2}R_2 s(\gamma)s(\alpha)\\ \rho_2 s(\theta_2) + \frac{1}{2}R_2 s(\gamma) + \frac{\sqrt{3}}{2}R_2 c(\gamma)s(\alpha)\\ \frac{\sqrt{3}}{2}\rho_2 c(\theta_2) + \frac{\sqrt{3}}{2}s_2 - \frac{\sqrt{3}}{2}R_2 c(\alpha)\end{bmatrix} \\
= \;& -2\left(\rho_2 s(\theta_2) + \frac{1}{2}R_2 s(\gamma) + \frac{\sqrt{3}}{2}R_2 c(\gamma)s(\alpha)\right) \\
= \;& -R_2\left(s(\gamma) + \sqrt{3}c(\gamma)s(\alpha)\right) - 2\rho_2 s(\theta_2) \\
= \;& -R\left(\frac{2t_\gamma}{1 + t_\gamma^2} + 2\sqrt{3}\left(\frac{1 - t_\gamma^2}{1 + t_\gamma^2}\right)\left(\frac{t_\alpha}{1 + t_\alpha^2}\right)\right) - 2\rho s(\theta_2) \\
= \;& -R\frac{1}{1 + t_\gamma^2}\left(2t_\gamma + 2\sqrt{3}\frac{t_\alpha\big(1 - t_\gamma^2\big)}{(1 + t_\alpha^2)}\right) - 2\rho s(\theta_2)
\end{aligned}
$$

Next, B_2 is determined:

$$
\begin{aligned}
B_2 = \;& 2\boldsymbol{s_2}^{\mathrm{T}}(\boldsymbol{\rho_2} - \boldsymbol{R_2}) - 2\boldsymbol{\rho_2}^{\mathrm{T}}\boldsymbol{R_2} + c_2 \\
= \;& 2\begin{bmatrix} -\frac{1}{2}s_2 & 0 & \frac{\sqrt{3}}{2}s_2 \end{bmatrix}\left(\begin{bmatrix} -\frac{1}{2}\rho_2 c(\theta_2) \\ \rho_2 s(\theta_2) \\ \frac{\sqrt{3}}{2}\rho_2 c(\theta_2) \end{bmatrix} - \begin{bmatrix} -\frac{1}{2}R_2 c(\gamma) + \frac{\sqrt{3}}{2}R_2 s(\gamma)s(\alpha) \\ -\frac{1}{2}R_2 s(\gamma) - \frac{\sqrt{3}}{2}R_2 c(\gamma)s(\alpha) \\ \frac{\sqrt{3}}{2}R_2 c(\alpha) \end{bmatrix}\right) \\
& - 2\begin{bmatrix} -\frac{1}{2}\rho_2 c(\theta_2) & \rho_2 s(\theta_2) & \frac{\sqrt{3}}{2}\rho_2 c(\theta_2) \end{bmatrix}\begin{bmatrix} -\frac{1}{2}R_2 c(\gamma) + \frac{\sqrt{3}}{2}R_2 s(\gamma)s(\alpha) \\ -\frac{1}{2}R_2 s(\gamma) - \frac{\sqrt{3}}{2}R_2 c(\gamma)s(\alpha) \\ \frac{\sqrt{3}}{2}R_2 c(\alpha) \end{bmatrix} + c_2 \\
= \;& \begin{bmatrix} -s_2 & 0 & \sqrt{3}s_2 \end{bmatrix}\begin{bmatrix} -\frac{1}{2}\rho_2 c(\theta_2) + \frac{1}{2}R_2 c(\gamma) - \frac{\sqrt{3}}{2}R_2 s(\gamma)s(\alpha) \\ \rho_2 s(\theta_2) + \frac{1}{2}R_2 s(\gamma) + \frac{\sqrt{3}}{2}R_2 c(\gamma)s(\alpha) \\ \frac{\sqrt{3}}{2}\rho_2 c(\theta_2) - \frac{\sqrt{3}}{2}R_2 c(\alpha) \end{bmatrix} \\
& + \begin{bmatrix} \rho_2 c(\theta_2) & -2\rho_2 s(\theta_2) & -\sqrt{3}\rho_2 c(\theta_2) \end{bmatrix}\begin{bmatrix} -\frac{1}{2}R_2 c(\gamma) + \frac{\sqrt{3}}{2}R_2 s(\gamma)s(\alpha) \\ -\frac{1}{2}R_2 s(\gamma) - \frac{\sqrt{3}}{2}R_2 c(\gamma)s(\alpha) \\ \frac{\sqrt{3}}{2}R_2 c(\alpha) \end{bmatrix} + c_2 \\
= \;& -s_2\left(-\frac{1}{2}\rho_2 c(\theta_2) + \frac{1}{2}R_2 c(\gamma) - \frac{\sqrt{3}}{2}R_2 s(\gamma)s(\alpha)\right) + \sqrt{3}s_2\left(\frac{\sqrt{3}}{2}\rho_2 c(\theta_2) - \frac{\sqrt{3}}{2}R_2 c(\alpha)\right) \\
& + \rho_2 c(\theta_2)\left(-\frac{1}{2}R_2 c(\gamma) + \frac{\sqrt{3}}{2}R_2 s(\gamma)s(\alpha)\right) - 2\rho_2 s(\theta_2)\left(-\frac{1}{2}R_2 s(\gamma) - \frac{\sqrt{3}}{2}R_2 c(\gamma)s(\alpha)\right) \\
& - \sqrt{3}\rho_2 c(\theta_2)\left(\frac{\sqrt{3}}{2}R_2 c(\alpha)\right) + c_2
\end{aligned}
$$

After further rearranging and simplification, this can be simplified to:

$$
\begin{aligned}
B_2 = \;& -\tfrac{1}{2}R\big(s + \rho c(\theta_2)\big)\Big(c(\gamma) + 3c(\alpha) - \sqrt{3}s(\gamma)s(\alpha)\Big) + \rho R s(\theta_2)s(\gamma) + \\
& \sqrt{3}R\rho s(\theta_2)c(\gamma)s(\alpha) + 2s\rho c(\theta_2) + c_2 \\
= \;& -\tfrac{1}{2}R\big(s + \rho c(\theta_2)\big)\left(\tfrac{1-t_\gamma^2}{1+t_\gamma^2} + 3\tfrac{1-t_\alpha^2}{1+t_\alpha^2} - 4\sqrt{3}\tfrac{t_\gamma t_\alpha}{(1+t_\gamma^2)(1+t_\alpha^2)}\right) + 2\rho R s(\theta_2)\tfrac{t_\gamma}{1+t_\gamma^2} + \\
& 2\sqrt{3}R\rho s(\theta_2)\tfrac{t_\alpha(1-t_\gamma^2)}{(1+t_\gamma^2)(1+t_\alpha^2)} + 2s\rho c(\theta_2) - l^2 + \rho + R^2 + s^2
\end{aligned}
$$

Next, A_3 is determined:

$$
\begin{aligned}
A_3 = \;& -2\boldsymbol{n}^{\mathrm{T}}(\boldsymbol{\rho_3} + \boldsymbol{s_3} - \boldsymbol{R_3}) \\
= \;& -2[0 \quad 1 \quad 0]\left(\begin{bmatrix} -\frac{1}{2}\rho_3 c(\theta_3) \\ \rho_3 s(\theta_3) \\ -\frac{\sqrt{3}}{2}\rho_3 c(\theta_3) \end{bmatrix} + \begin{bmatrix} -\frac{1}{2}s_3 \\ 0 \\ -\frac{\sqrt{3}}{2}s_3 \end{bmatrix} - \begin{bmatrix} -\frac{1}{2}R_3 c(\gamma) - \frac{\sqrt{3}}{2}R_3 s(\gamma)s(\alpha) \\ -\frac{1}{2}R_3 s(\gamma) + \frac{\sqrt{3}}{2}R_3 c(\gamma)s(\alpha) \\ -\frac{\sqrt{3}}{2}R_3 c(\alpha) \end{bmatrix}\right) \\
= \;& [0 \quad -2 \quad 0]\begin{bmatrix} -\frac{1}{2}\rho_3 c(\theta_3) - \frac{1}{2}s_3 + \frac{1}{2}R_3 c(\gamma) + \frac{\sqrt{3}}{2}R_3 s(\gamma)s(\alpha) \\ \rho_3 s(\theta_3) + \frac{1}{2}R_3 s(\gamma) - \frac{\sqrt{3}}{2}R_3 c(\gamma)s(\alpha) \\ -\frac{\sqrt{3}}{2}\rho_3 c(\theta_3) - \frac{\sqrt{3}}{2}s_3 + \frac{\sqrt{3}}{2}R_3 c(\alpha) \end{bmatrix} \\
= \;& -2\left(\rho_3 s(\theta_3) + \frac{1}{2}R_3 s(\gamma) - \frac{\sqrt{3}}{2}R_3 c(\gamma)s(\alpha)\right) \\
= \;& R_3\left(-s(\gamma) + \sqrt{3}c(\gamma)s(\alpha)\right) - 2\rho_3 s(\theta_3) \\
= \;& R\left(-\frac{2t_\gamma}{1+t_\gamma^2} + 2\sqrt{3}\left(\frac{1-t_\gamma^2}{1+t_\gamma^2}\right)\left(\frac{t_\alpha}{1+t_\alpha^2}\right)\right) - 2\rho s(\theta_3) \\
= \;& -R\frac{1}{1+t_\gamma^2}\left(2t_\gamma - 2\sqrt{3}\frac{t_\alpha\left(1-t_\gamma^2\right)}{(1+t_\alpha^2)}\right) - 2\rho s(\theta_3)
\end{aligned}
$$

Finally, B_3 is determined:

$$
\begin{aligned}
B_3 = \;& 2\boldsymbol{s_3}^{\mathrm{T}}(\boldsymbol{\rho_3} - \boldsymbol{R_3}) - 2\boldsymbol{\rho_3}^{\mathrm{T}}\boldsymbol{R_3} + c_3 \\
= \;& 2\left[-\frac{1}{2}s_3 \quad 0 \quad -\frac{\sqrt{3}}{2}s_3\right]\left(\begin{bmatrix} -\frac{1}{2}\rho_3 c(\theta_3) \\ \rho_3 s(\theta_3) \\ -\frac{\sqrt{3}}{2}\rho_3 c(\theta_3) \end{bmatrix} - \begin{bmatrix} -\frac{1}{2}R_3 c(\gamma) - \frac{\sqrt{3}}{2}R_3 s(\gamma)s(\alpha) \\ -\frac{1}{2}R_3 s(\gamma) + \frac{\sqrt{3}}{2}R_3 c(\gamma)s(\alpha) \\ -\frac{\sqrt{3}}{2}R_3 c(\alpha) \end{bmatrix}\right) \\
& - 2\left[-\frac{1}{2}\rho_3 c(\theta_3) \quad \rho_3 s(\theta_3) \quad -\frac{\sqrt{3}}{2}\rho_3 c(\theta_3)\right]\begin{bmatrix} -\frac{1}{2}R_3 c(\gamma) - \frac{\sqrt{3}}{2}R_3 s(\gamma)s(\alpha) \\ -\frac{1}{2}R_3 s(\gamma) + \frac{\sqrt{3}}{2}R_3 c(\gamma)s(\alpha) \\ -\frac{\sqrt{3}}{2}R_3 c(\alpha) \end{bmatrix} + c_3
\end{aligned}
$$

$$= \begin{bmatrix} -s_3 & 0 & -\sqrt{3}s_3 \end{bmatrix} \begin{bmatrix} -\frac{1}{2}\rho_3 c(\theta_3) + \frac{1}{2}R_3 c(\gamma) + \frac{\sqrt{3}}{2}R_3 s(\gamma)s(\alpha) \\ \rho_3 s(\theta_3) + \frac{1}{2}R_3 s(\gamma) - \frac{\sqrt{3}}{2}R_3 c(\gamma)s(\alpha) \\ -\frac{\sqrt{3}}{2}\rho_3 c(\theta_3) + \frac{\sqrt{3}}{2}R_3 c(\alpha) \end{bmatrix} +$$

$$\begin{bmatrix} \rho_3 c(\theta_3) & -2\rho_3 s(\theta_3) & \sqrt{3}\rho_3 c(\theta_3) \end{bmatrix} \begin{bmatrix} -\frac{1}{2}R_3 c(\gamma) - \frac{\sqrt{3}}{2}R_3 s(\gamma)s(\alpha) \\ -\frac{1}{2}R_3 s(\gamma) + \frac{\sqrt{3}}{2}R_3 c(\gamma)s(\alpha) \\ -\frac{\sqrt{3}}{2}R_3 c(\alpha) \end{bmatrix} + c_3$$

$$= -s_3\left(-\frac{1}{2}\rho_3 c(\theta_3) + \frac{1}{2}R_3 c(\gamma) + \frac{\sqrt{3}}{2}R_3 s(\gamma)s(\alpha)\right) - \sqrt{3}s_2\left(-\frac{\sqrt{3}}{2}\rho_3 c(\theta_3) + \frac{\sqrt{3}}{2}R_3 c(\alpha)\right) +$$

$$\rho_3 c(\theta_3)\left(-\frac{1}{2}R_3 c(\gamma) - \frac{\sqrt{3}}{2}R_3 s(\gamma)s(\alpha)\right) - 2\rho_3 s(\theta_3)\left(-\frac{1}{2}R_3 s(\gamma) + \frac{\sqrt{3}}{2}R_3 c(\gamma)s(\alpha)\right) +$$

$$\sqrt{3}\rho_3 c(\theta_3)\left(-\frac{\sqrt{3}}{2}R_3 c(\alpha)\right) + c_3$$

After further rearranging and simplification, this can be simplified to:

$$B_3 = -\frac{1}{2}R\big(s + \rho c(\theta_3)\big)\Big(c(\gamma) + 3c(\alpha) + \sqrt{3}s(\gamma)s(\alpha)\Big) + \rho R s(\theta_3)s(\gamma) -$$

$$\sqrt{3}R\rho s(\theta_3)c(\gamma)s(\alpha) + 2s\rho c(\theta_3) + c_2$$

$$= -\frac{1}{2}R\big(s + \rho c(\theta_3)\big)\left(\frac{1-t_\gamma^2}{1+t_\gamma^2} + 3\frac{1-t_\alpha^2}{1+t_\alpha^2} + 4\sqrt{3}\frac{t_\gamma t_\alpha}{(1+t_\gamma^2)(1+t_\alpha^2)}\right) + 2\rho R s(\theta_3)\frac{t_\gamma}{1+t_\gamma^2} -$$

$$2\sqrt{3}R\rho s(\theta_3)\frac{t_\alpha(1-t_\gamma^2)}{(1+t_\gamma^2)(1+t_\alpha^2)} + 2s\rho c(\theta_3) - l^2 + \rho + R^2 + s^2$$

This completes the definition of the problem. To reiterate, we have Eq. 12 and Eq.13:

$$0 = A_1A_2(B_1 + B_2) - B_1(A_2^2 + B_1) - B_2(A_1^2 + B_2) + 2B_1B_2 \qquad \textit{Equation 12}$$

$$0 = A_2A_3(B_2 + B_3) - B_2(A_3^2 + B_2) - B_3(A_2^2 + B_3) + 2B_2B_3 \qquad \textit{Equation 13}$$

Where A_i and B_i for $i = 1, 2, 3$ have been defined. These equations must be solved simultaneously. A problem-based numerical approach using MATLAB's optimisation library was used to solve this system of nonlinear equations for the unknown angles γ and α. After solving for these, their values were used to calculate the values of A_1 and B_1, which can be used to solve Eq. 6 where $i = 1$, for H as shown below, using the quadratic formula.

$$0 = H^2 + A_1H + B_1 \qquad \textit{Equation 6.1}$$

This analysis was carried out in a custom MATLAB function called CALCSWASHDIRECT. An Excel plugin was also created so it could be used in Microsoft Excel. The MATLAB files and Microsoft Excel plugin have been provided along with this report. The code is also shown in Figure A.0.2 of Appendix A. This function takes the design parameters of the system, as well as the three servo angles as the inputs.

4.5.2 Up – SP Module (Direct kinematics)

For the UP – SP module, the direct kinematics should be able to calculate the blade pitch angle for the given collective input (which is dependent on H). A diagram of how the UP-SP module reacts to a collective input is shown in Figure 4.11. Only one blade is shown as collective input is symmetrical on both blades.

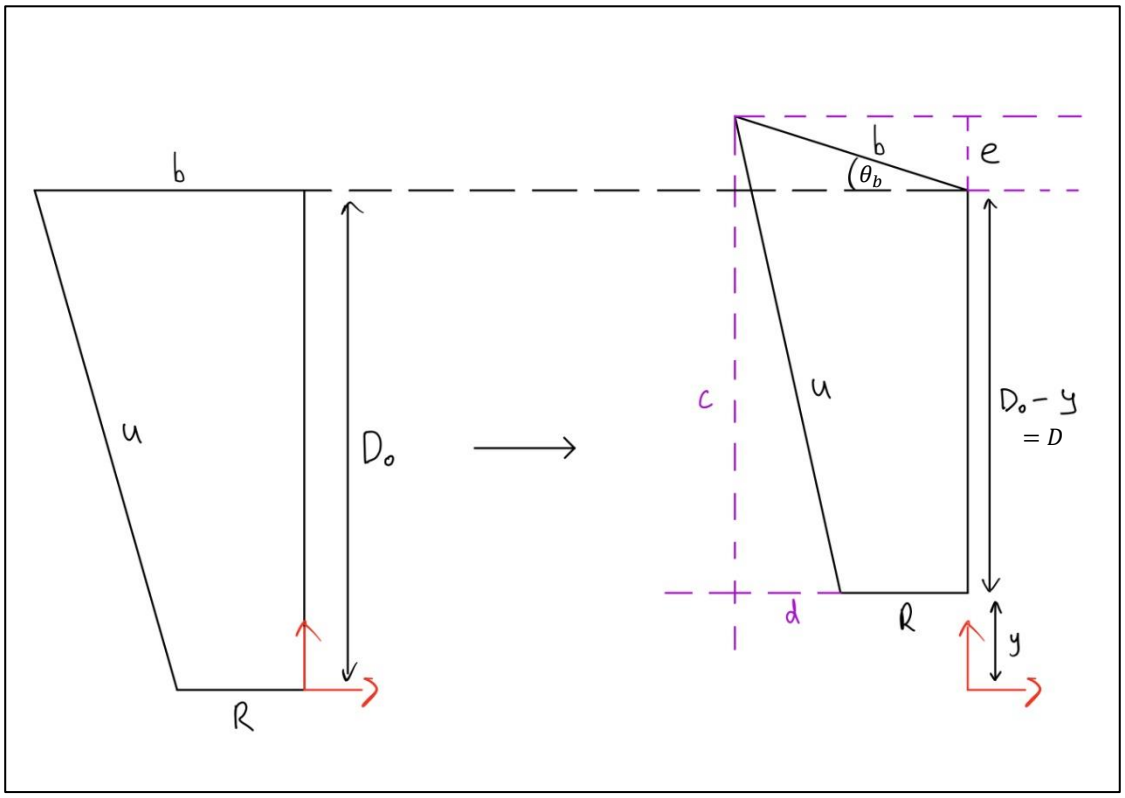

Figure 4.11: UP-SP module reacting to a collective input.

Since b, u and R are design parameters that are dependent on the Align T-Rex 550E Pro DFC rotor head design, D_0 could be calculated as follows:

$$D_0 = \sqrt{u^2 - (b - R)^2} \qquad \textit{Equation 14}$$

Given a specific collective input y, the blade angle θ_b must be found. As the pitch arm length is fixed:

$$\begin{aligned} u^2 &= c^2 + d^2 \\ &= (D_0 - y + e)^2 + d^2 \\ &= (D_0 - y + e)^2 + d^2 \\ &= (D_0 - y + b\sin\theta_B)^2 + (b\cos\theta_b - R)^2 \\ &= D_0^2 + y^2 + b^2 + R^2 - 2D_0 y + \sin\theta_B\,(2D_0 b - 2by) - 2Rb\cos\theta_b \end{aligned} \qquad \textit{Equation 15}$$

The following constants can be defined:

$$G = u^2 - (D_0^2 + y^2 + b^2 + R^2 - 2D_0 y)$$

$$K = (2D_0 b - 2by)$$

$$T = 2Rb$$

Also following half-tangent relations can be used:

$$s(\theta_b) = \frac{2t_{\theta_b}}{1+t_{\theta_b}^2}, \qquad c(\theta_b) = \frac{1-t_{\theta_b}^2}{1+t_{\theta_b}^2}, \qquad \text{Where, } t_{\theta_b} = \tan\left(\frac{\theta_b}{2}\right)$$

Applying the above to Eq. 15 gives:

$$\begin{aligned} G &= K\sin\theta_B - T\cos\theta_b \\ &= \frac{2Kt_{\theta_b}}{1+t_{\theta_b}^2} - \frac{T\left(1-t_{\theta_b}^2\right)}{1+t_{\theta_b}^2} = \frac{2Kt_{\theta_b} - T\left(1-t_{\theta_b}^2\right)}{1+t_{\theta_b}^2} \end{aligned}$$

After further simplification, this can be rearranged to:

$$0 = (T-G)t_{\theta_b}^2 + 2Kt_{\theta_b} - (T+G) \qquad \textit{Equation 16}$$

Eq. 16 can be solved for t_{θ_b} using the quadratic formula:

$$\begin{aligned} t_{\theta_b} &= \frac{-2K \pm \sqrt{4K^2 + 4(T-G)(T+G)}}{2(T+G)} \\ &= \frac{K \pm \sqrt{K^2 + (T^2 - G^2)}}{(G-T)} \end{aligned} \qquad \textit{Equation 17}$$

Finally, using the definition for t_{θ_b}, θ_b can be calculated:

$$\theta_b = 2\arctan\left(\frac{K \pm \sqrt{K^2 + (T^2 - G^2)}}{(G-T)}\right) \qquad \textit{Equation 18}$$

Eq. 18 can be used to calculate the blade angle given a specific collective input.

4.5.3 Global direct kinematics model

The direct kinematics model for both the Down-SP and Up-SP module have been derived. To produce a global direct kinematics model, a MS Excel sheet was developed. This section will explain how the equations developed in the previous sections are used in the MS Excel sheet. The MS Excel sheet is provided along with this report (multiple MS Excel sheets are added, depending on the design constraints used).

As shown in Figure 4.12, the top left section of each MS Excel sheet has the geometry values. The cells highlighted yellow are the changeable design factors. The servo angle to blade angle scale factor was also added as another parameter to allow for more solutions to the optimisation problem instead of having just a one to one relationship between the servo angle input and the blade angle output.

	A	B
1	Geometry Values / mm	
2	R*	24.36
3	u	53.965
4	b	27.822
5		
6	s1	
7	s2	
8	s3	
9	s	30
10		
11	ρ1	
12	ρ2	
13	ρ3	
14	ρ	17
15		
16	L1	
17	L2	
18	L3	
19	L	45
20		
21	R	38.451
22		
23		
24	D0	53.8538372
25	D1	51.43031346
26	D2	49.04580258
27	D3	46.69680406
28		
29		
30	Servo angle to blade angle scale factor	1.604808676
31		
32		
33	H - initial	44.18047758

Figure 4.12: Input section of the MS Excel file

D_0 is calculated using Eq. 14, whilst $H_{initial}$ is calculated using the CALCSWASHDIRECT function with the following design parameters and the initial servo angles which are all set to zero. This function returns a row vector with the swash tilt angles, α, γ and H. Therefore, the INDEX function is needed to extract H. The code used in cell B33 is:

=INDEX(CALCSWASHDIRECT(B21,B14,B19,B9,0,0,0),1,3)

	E	F	G	H	I
1	Direct Kinematics				
2					
3					
4					
5	**Blade Angle (Degrees)**	**Servo Angle 1 (Degrees)**	**Servo Angle 2 (Degrees)**	**Servo Angle 3 (Degrees)**	**Calculated H**
6	-15	-24.07213014	-24.07213014	-24.07213014	37.50698492
7	-14	-22.46732146	-22.46732146	-22.46732146	37.91405837
8	-13	-20.86251279	-20.86251279	-20.86251279	38.32747631
9	-12	-19.25770411	-19.25770411	-19.25770411	38.74706421
10	-11	-17.65289543	-17.65289543	-17.65289543	39.17263401
11	-10	-16.04808676	-16.04808676	-16.04808676	39.60398375
12	-9	-14.44327808	-14.44327808	-14.44327808	40.04089723
13	-8	-12.83846941	-12.83846941	-12.83846941	40.48314374
14	-7	-11.23366073	-11.23366073	-11.23366073	40.93047779
15	-6	-9.628852055	-9.628852055	-9.628852055	41.38263892
16	-5	-8.024043379	-8.024043379	-8.024043379	41.83935156
17	-4	-6.419234704	-6.419234704	-6.419234704	42.30032494
18	-3	-4.814426028	-4.814426028	-4.814426028	42.76525303
19	-2	-3.209617352	-3.209617352	-3.209617352	43.2338146
20	-1	-1.604808676	-1.604808676	-1.604808676	43.70567325
21	0	0	0	0	44.18047758
22	1	1.604808676	1.604808676	1.604808676	44.65786138
23	2	3.209617352	3.209617352	3.209617352	45.1374439
24	3	4.814426028	4.814426028	4.814426028	45.61883017
25	4	6.419234704	6.419234704	6.419234704	46.10161139
26	5	8.024043379	8.024043379	8.024043379	46.58536535
27	6	9.628852055	9.628852055	9.628852055	47.06965697
28	7	11.23366073	11.23366073	11.23366073	47.55403885
29	8	12.83846941	12.83846941	12.83846941	48.03805187
30	9	14.44327808	14.44327808	14.44327808	48.52122588
31	10	16.04808676	16.04808676	16.04808676	49.00308039
32	11	17.65289543	17.65289543	17.65289543	49.4831254
33	12	19.25770411	19.25770411	19.25770411	49.96086215
34	13	20.86251279	20.86251279	20.86251279	50.43578397
35	14	22.46732146	22.46732146	22.46732146	50.90737723
36	15	24.07213014	24.07213014	24.07213014	51.3751222

Figure 4.13: Calculating the actual swash height

Initially, the design parameters highlighted yellow in Figure 4.12 are guessed. The guessed servo to blade angle scale factor is used to calculate the input servo angles as shown in Figure 4.13, where the servo angle is the ideal blade angle multiplied by the scale factor. These are used to calculate H using the CALCSWASHDIRECT function.

To relate the results from the Down-SP module (i.e. the calculated H), the parameter D as shown in Figure 4.11 is calculated as follows:

$$D = D_0 - (H - H_0) \qquad \textit{Equation 19}$$

This is used to calculate the distance between the swashplate and the blade mounting point which can be used with the equations found in the direct kinematics of the UP-SP module.

	J	K	L	M	N	O	P	Q
5	Calculated D	G	K	T	Blade Angle	Ideal	Difference	Blade Angle Deviation Sum Positive (degrees)
6	60.52732985	-2118.809718	3367.982742	1355.48784	**-13.78197105**	-15	-1.218028949	1.218028949
7	60.12025641	-2069.69729	3345.331548	1355.48784	**-12.93050407**	-14	-1.069495933	1.069495933
8	59.70683847	-2020.158619	3322.32732	1355.48784	**-12.06838238**	-13	-0.931617622	0.931617622
9	59.28725057	-1970.230139	3298.979771	1355.48784	**-11.19580168**	-12	-0.804198323	0.804198323
10	58.86168077	-1919.949522	3275.299365	1355.48784	**-10.31296941**	-11	-0.687030586	0.687030586
11	58.43033103	-1869.355643	3251.29734	1355.48784	**-9.420105989**	-10	-0.579894011	0.579894011
12	57.99341754	-1818.488537	3226.985726	1355.48784	**-8.517445974**	-9	-0.482554026	0.482554026
13	57.55117103	-1767.389346	3202.377361	1355.48784	**-7.60523935**	-8	-0.39476065	0.39476065
14	57.10383699	-1716.100258	3177.485905	1355.48784	**-6.683752758**	-7	-0.316247242	0.316247242
15	56.65167586	-1664.664437	3152.325852	1355.48784	**-5.753270776**	-6	-0.246729224	0.246729224
16	56.19496322	-1613.12595	3126.912533	1355.48784	**-4.814097208**	-5	-0.185902792	0.185902792
17	55.73398984	-1561.529682	3101.262131	1355.48784	**-3.866556385**	-4	-0.133443615	0.133443615
18	55.26906174	-1509.921245	3075.391672	1355.48784	**-2.910994489**	-3	-0.089005511	0.089005511
19	54.80050017	-1458.346878	3049.319032	1355.48784	**-1.947780885**	-2	-0.052219115	0.052219115
20	54.32864153	-1406.853349	3023.062929	1355.48784	**-0.977309465**	-1	-0.022690535	0.022690535
21	53.8538372	-1355.48784	2996.642917	1355.48784	**0**	0	0	0
22	53.3764534	-1304.297836	2970.079373	1355.48784	**0.983700504**	1	0.016299496	0.016299496
23	52.89687088	-1253.331008	2943.393483	1355.48784	**1.973316445**	2	0.026683555	0.026683555
24	52.4154846	-1202.635085	2916.607225	1355.48784	**2.968342277**	3	0.031657723	0.031657723
25	51.93270339	-1152.25774	2889.743347	1355.48784	**3.968241159**	4	0.031758841	0.031758841
26	51.44894943	-1102.246456	2862.825342	1355.48784	**4.972443638**	5	0.027556362	0.027556362
27	50.9646578	-1052.648404	2835.877419	1355.48784	**5.980346339**	6	0.019653661	0.019653661
28	50.48027592	-1003.510316	2808.924473	1355.48784	**6.991310705**	7	0.008689295	0.008689295
29	49.9962629	-954.8783634	2781.992053	1355.48784	**8.004661771**	8	-0.004661771	0.004661771
30	49.5130889	-906.7980315	2755.106319	1355.48784	**9.019687003**	9	-0.019687003	0.019687003
31	49.03123438	-859.3140042	2728.294006	1355.48784	**10.0356352**	10	-0.035635196	0.035635196
32	48.55118937	-812.4700485	2701.582381	1355.48784	**11.05171547**	11	-0.051715472	0.051715472
33	48.07345263	-766.3089068	2674.999198	1355.48784	**12.06709637**	12	-0.067096365	0.067096365
34	47.5985308	-720.8721937	2648.572648	1355.48784	**13.08090503**	13	-0.080905031	0.080905031
35	47.12693754	-676.2003012	2622.331313	1355.48784	**14.09222659**	14	-0.092226594	0.092226594
36	46.65919257	-632.3323107	2596.304112	1355.48784	**15.10010365**	15	-0.100103649	0.100103649
37								
38							**Deviation Sum**	**7.828148147**

Figure 4.15: Calculating the blade pitch angle

As shown in Figure 4.14, the scalar coefficients G, K *and* T from Eq. 18 can be calculated. These can be used to calculate the actual blade angle highlighted yellow in Figure 4.14. These parameters can be used to calculate the overall deviation sum between the ideal pitch curve and the actual pitch curve, which is also shown in Figure 4.14. The optimisation problem will minimise this deviation sum.

The deviation sum was calculated only in the positive region as this is the region that UAV helicopters operate in.

To start the solving process, once the Excel Solver plug in is enabled and the CALCSWASH-DIRECT plugin is imported, the Solver function can be accessed from the Data panel of MS Excel.

The constraints used are summarised in Table 1 and 2 on the next page. All parameters were constrained to be non-negative.

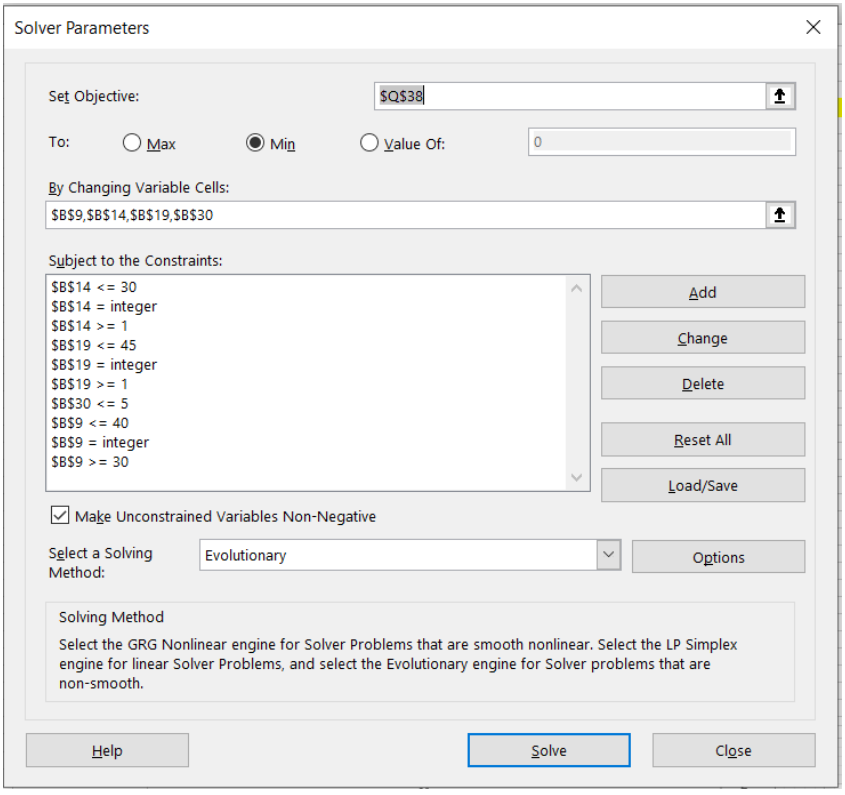

Figure 4.14: MS Excel Solver setup

Parameter	Constraint 1	Constraint 2	Constraint 3
s = servo motor mounting distance	$s \geq$ 30mm. 30mm is the closest the servos can be placed from the main shaft whilst being clear from the swashplate movement.	A max value was arbitrarily set to 40mm.	Integer only.
ρ = servo horn length	$\rho \leq$ 30mm. This was chosen to keep the design small. Original design was 24.05mm	Integer only	-
L = linkage arm length	$L \leq$ 45mm. Original design was 45mm	Integer only	-
Servo angle to blade angle scale factor	Servo angle to blade angle scale factor $\leq$ 5. An arbitrary maximum was set to complete the constraints	-	-

Table 1: Optimisation problem 1 – constraints

Parameter	Constraint 1	Constraint 2	Constraint 3
s = servo motor mounting distance	$s \geq$ 30mm. 30mm is the closest the servos can be placed from the main shaft whilst being clear from the swashplate movement.	A max value was arbitrarily set to 40mm.	-
ρ = servo horn length	$\rho \leq$ 30mm. This was chosen to keep the design small. Original design was 24.05mm	-	-
L = linkage arm length	$L \leq$ 80mm.	-	-
Servo angle to blade angle scale factor	Servo angle to blade angle scale factor $\leq$ 5. An arbitrary maximum was set to complete the constraints	-	-

Table 2: Optimisation problem 2 - constraints

Problem 2 was set to see the impact of having an integer only solution, and a larger range for L.

5 Results:

5.1 Results from MS Excel

After running the Solver, the calculated design parameters were found to be:

Parameter	Calculated Value – Problem 1	Calculated Value – Problem 2
s = servo motor mounting distance	30	30
ρ = servo horn length	17	17.1449487
L = linkage arm length	45	80
Servo angle to blade angle scale factor	1.604808676	1.604808676

Table 3: Solution of the optimisation problem.

Using the global kinematic model to calculate the blade angles, the pitch curves of these solutions are shown in below.

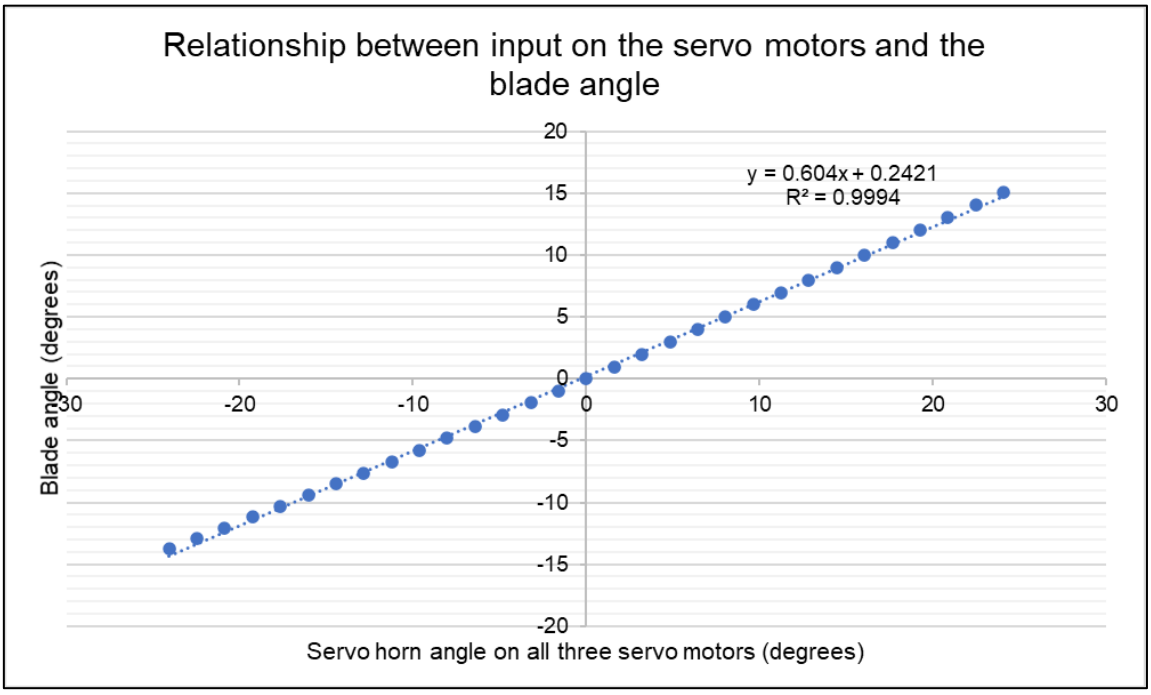

Figure 5.1: Pitch curve for the solution to problem 1.

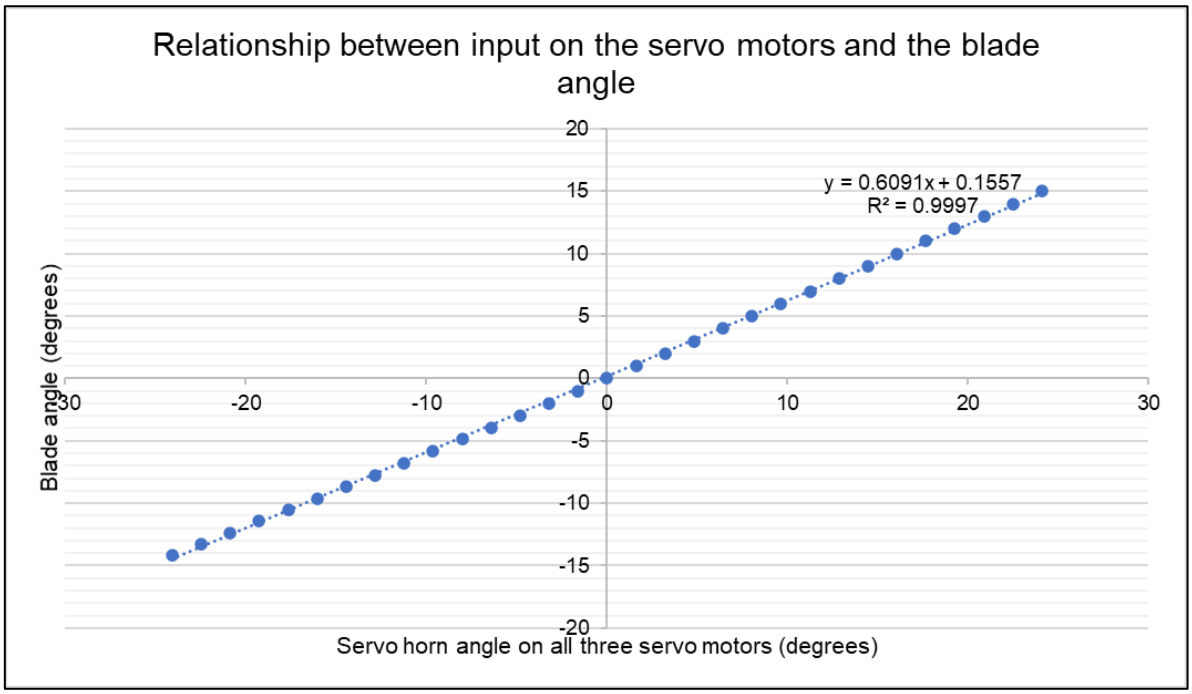

Figure 5.2: Pitch curve for the solution to problem 2.

The characteristic values from these graphs can be compared to those plotted for the Align T-Rex 550E Pro DFC Rotor head system.

	Align T-Rex 550E Pro DFC	Solution to Problem 1	Solution to Problem 2
Gradient	0.7295	0.604	0.6091
Coefficient of determination (R^2)	0.9995	0.9994	0.9997

Table 4: Comparing results of the new design to the old design.

6 Conclusions and future work:

From the results, it is evident that the new design from problem 1 has slight drop in the coefficient of determination than the original design. However, the solution to problem 2 provided a slight increase in the coefficient of determination. Though this drop and increase is very minimal, the key thing to note was the improvement in the design in respect to a better force transfer due to the new servo arrangement. The solution from problem 1 was able to produce an almost equivalent design in terms of linearity, whilst improving the servo arrangement to account better for the dynamics of the system.

The solution from problem 2 shows that the results are a function of the constraints of the problem. To achieve a design closer to the system, the constraints can be changed, however, this is a choice of the designer, after considering the other components that are to be added to the RC helicopter.

This analysis has shown that using an optimisation algorithm in conjunction with a kinematic model of an RC helicopter system provides a suitable method to producing and analysing prototype designs. It has also been a good method for improving existing rotor head systems, by finding alternative design parameters that can be easily changed, to improve its mechanical behaviour.

In the future, this work could be used to inspire engineers for future research in prototyping designs that can produce the pitch curve needed to match the thrust curve of a specific set of rotor-blades, or produce a pitch curve that achieves the desired roll rates for cyclic inputs. This would require the use of integrating the global kinematic model with a fluids model, such as the one developed by Stephen Bell using blade element momentum theory. (15)

References:

1. WorthPoint. ALIGN T-Rex 550E Pro DFC rotor head system No Date [Available from: https://thumbs.worthpoint.com/zoom/images1/1/1113/26/complete-align-600dfc-main-rotor-head_1_23bd1264b323bc44226f7db28495ebda.jpg.
2. Yuan X, Zhu J, Chen Z, Lu X, Meng J. Comprehensive kinematic modeling and analysis of a coaxial helicopter's swashplate mechanism. Proceedings of the Institution of Mechanical Engineers, Part C: Journal of Mechanical Engineering Science. 2015;229(10):1839-60.
3. Zhang C, Chen Y, Xu H, Hu M, Zhang R. Kinematic modeling and dexterity evaluation of a PS-RRS-2RUS parallel manipulator used for controllable pitch propeller. Mechanics Based Design of Structures and Machines. 2018;46(5):533-51.
4. Sabaapour MR, Zohoor H. Analysis of a Swashplate Mechanism of the Hingeless Rotor Hub with the Flybar in a Model Helicopter, Part I: Kinematics. Journal of System Design and Dynamics. 2010;4(4):616-31.
5. Salt J. Understanding Flybarless RC Helicopters 2019 [Available from: https://www.rchelicopterfun.com/flybarless.html.
6. Hintz T. Align T-Rex 550E PRO DFC 2013 [Available from: https://www.flyingrc.net/trex550epro.html.
7. Stevens BL. Aircraft control and simulation : dynamics, controls design, and autonomous systems / Brian L. Stevens, Frank L. Lewis, Eric N. Johnson. Third edition. ed. Lewis FL, Johnson EN, editors: Hoboken, New Jersey : Wiley; 2015.
8. Limited SHT. Instructions v2.3 SOKO KIT Auckland: Soko Heli Tools Limited; 2013 [
9. Corporation F. Flybarless Control Gyro - CGY750 Instruction Manual V1.40 ~ Japan2013 [Available from: http://manuals.hobbico.com/fut/cgy750-manual.pdf.
10. T-REX 550E PRO DFC [Internet]. 2017 [cited 12/05/2020]. Available from: https://grabcad.com/library/t-rex-550e-pro-dfc-1.
11. Smith S, Lasdon L. Solving Large Sparse Nonlinear Programs Using GRG. ORSA Journal on Computing. 1992;4(1):2.
12. Frontline Systems I. EXCEL SOLVER - NON-SMOOTH OPTIMIZATION 2020 [Available from: https://www.solver.com/excel-solver-non-smooth-optimization.
13. Young C. EXCEL SOLVER: WHICH SOLVING METHOD SHOULD I CHOOSE? : EngineerExcel.com; 2020 [Available from: https://www.engineerexcel.com/excel-solver-solving-method-choose/.
14. Thomas Grossman AL. Meta-Heuristic Solvers [Website]. San Francisco: University of San Francisco's School of Business and Professional Studies; [updated May 3, 2010. 3:[Available from: https://sites.google.com/a/usfca.edu/business-analytics/model-driven-analytics/solvers/meta-heuristics.
15. Analysis of a Rotor Blade System using Blade Element Momentum Theory [Internet]. 2020 [cited 27/05/2020]. Available from: https://uk.mathworks.com/matlabcentral/fileexchange/21994-analysis-of-a-rotor-blade-system-using-blade-element-momentum-theory.

Appendix A:

a) b) c)

Figure A.0.1: Different flybarless configurations a) non-integrated washout type, b) integrated washout type and c) DFC or driverless head. (5)

```
function [swash] = CALCSWASHDIRECT(R,rho,L,s,theta1,theta2,theta3)

theta1 = deg2rad(theta1);
theta2 = deg2rad(theta2);
theta3 = deg2rad(theta3);

t = optimvar('t', 2);
% t(1) = t_gamma
% t(2) = t_alpha

A_1 = -2*rho*sin(theta1) + 4*R*(t(1)/(1+t(1)^2));

B_1 = (-2*R*(rho*cos(theta1) + s)*(1-t(1)^2) - 4*rho*R*sin(theta1)*t(1))/(1+t(1)^2) +
2*rho*s*cos(theta1) - L^2 + rho^2 + s^2 + R^2;

A_2 = ((-R)/(1+t(1)^2))*(2*t(1) + 2*sqrt(3)*t(2)*((1-t(1)^2)/(1+t(1)^2))) -
2*rho*sin(theta2);

B_2 = (((-R)*(s + rho*cos(theta2)))/2)*(((1-t(1)^2)/(1+t(1)^2)) + 3*((1-
t(2)^2)/(1+t(2)^2)) - 4*sqrt(3)*((t(1)*t(2))/((1+t(1)^2)*(1+t(2)^2)))) ...
+ 2*rho*R*sin(theta2)*(t(1)/(1+t(1)^2)) + 2*sqrt(3)*R*rho*sin(theta2)*t(2)*((1-
t(1)^2)/((1+t(1)^2)*(1+t(2)^2))) + 2*s*rho*cos(theta2) - L^2 + rho^2 + s^2 + R^2;

A_3 = ((-R)/(1+t(1)^2))*(2*t(1) - 2*sqrt(3)*t(2)*((1-t(1)^2)/(1+t(1)^2))) -
2*rho*sin(theta3);

B_3 = (((-R)*(s + rho*cos(theta3)))/2)*(((1-t(1)^2)/(1+t(1)^2)) + 3*((1-
t(2)^2)/(1+t(2)^2)) + 4*sqrt(3)*((t(1)*t(2))/((1+t(1)^2)*(1+t(2)^2)))) ...
+ 2*rho*R*sin(theta3)*(t(1)/(1+t(1)^2)) - 2*sqrt(3)*R*rho*sin(theta3)*t(2)*((1-
t(1)^2)/((1+t(1)^2)*(1+t(2)^2))) + 2*s*rho*cos(theta3) - L^2 + rho^2 + s^2 + R^2;

eq1 = A_1*A_2*(B_1+B_2) - B_1*(A_2^2 + B_1) - B_2*(A_1^2 + B_2) + 2*B_1*B_2 == 0;

eq2 = A_2*A_3*(B_2+B_3) - B_2*(A_3^2 + B_2) - B_3*(A_2^2 + B_3) + 2*B_2*B_3 == 0;

prob = eqnproblem;
prob.Equations.eq1 = eq1;
prob.Equations.eq2 = eq2;

%show(prob)

t0.t = [0 0];
```

```
[sol,fval,exitflag] = solve(prob,t0);

gamma = 2*atan(sol.t(1));
alpha = 2*atan(sol.t(2));

%disp("Gamma = " + rad2deg(gamma))
%disp("Alpha = " + rad2deg(alpha))

A_1 = -2*rho*sin(theta1) + 4*R*(gamma/(1+gamma^2));

B_1 = (-2*R*(rho*cos(theta1) + s)*(1-gamma^2) - 4*rho*R*sin(theta1)*gamma)/(1+gamma^2) +
2*rho*s*cos(theta1) - L^2 + rho^2 + s^2 + R^2;

p = [1 A_1 B_1];
r = roots(p);
q = size(r);

for i = 1:2
    if r(i) > 0
        H = r(i);
    end
end

swash = [rad2deg(gamma), rad2deg(alpha), H];

end
```

Figure A.0.2: CALCSWASHDIRECT MATLAB function code